Geophysical Journal (1989) **97**, 275–294

A low-velocity zone within the layer 3 region of 118 Myr old oceanic crust in the western North Atlantic

Rakesh Mithal and John C. Mutter*

Lamont-Doherty Geological Observatory of Columbia University, Palisades, NY 10964, USA

Accepted 1988 October 24. Received 1988 October 24; in original form 1987 January 8.

SUMMARY

During the North Atlantic transect (NAT) experiment 11 expanding spread profiles (ESPs) were acquired using a 3300 cubic inch, 30-element tuned airgun array (S/V *Prospekta*) and a 48-channel seismic streamer (R/V *Moore*). Extremely high-density seismograms were obtained that have allowed us to transform the observed data to the domain of intercept time and ray parameter (tau-p) with high precision. Velocity structures have been obtained by tau-sum inversion, ray tracing, and synthetic WKBJ and reflectivity seismogram methods both in tau-p and x-t domains.

A detailed analysis of ESP 5 suggests the presence of a low-velocity zone within the lower oceanic crust at the location of magnetic anomaly M0 (118 Ma). It is apparently 2.86 km thick, has a P-wave velocity of 6.5 km s^{-1}, S-wave velocity of 3.6 km s^{-1}, and occupies much of the depth interval normally associated with oceanic layer 3. Converted shear wave arrivals have been used to obtain the shear velocity structure. We find that the V_p/V_s ratio in the uppermost part of the crust is about 1.9, and much of the crustal section has a V_p/V_s ratio greater than $\sqrt{3}$. Attenuation of P- and S-waves has been studied by amplitude analysis, and we find that in most of the lower crust Q_s is equal to Q_p. Comparison with solutions from ESPs in younger and older parts of the basin suggests that ESP 5 is unique in displaying a low-velocity zone. Despite this the total thickness at ESP 5 is not significantly different than at other locations. We suggest that this provides strong evidence that the low-velocity zone occurs within the lower crust, and does not result from serpentinization of the upper mantle beneath thin oceanic crust.

Key words: converted shear waves, expanding spread profiles, Moho, North Atlantic, oceanic crust

INTRODUCTION

Much of our knowledge of the velocity structure of oceanic crust derives from analysis of seismic experiments that employed relatively large shot spacing, and thus the observed data are very sparse. Even the Fanfare data used by Spudich & Orcutt (1980a, b) to define detailed aspects of velocity structure have seismograms at an average spacing of 2.5 km. Solutions for crustal structure obtained using these data include up to 20 uniform-velocity or constant-gradient layers defining a structure that typically shows a monotonic increase in P-wave and S-wave velocity with depth [see White (1984) for instance]. The mineralogical assemblages that comprise the oceanic crust are complex, however, and subject to hydrothermal metamorphism following emplacement. Seismic velocities could decrease with depth in some parts of the oceanic crust without implying exotic crustal compositions. The effect of such a low-velocity zone in marine seismograms may be quite subtle and not easily recognized in the sparsely shot data upon which many models of crustal structure have been constructed.

The quantitative description of a low-velocity zone using standard traveltime inversion of seismic data is not possible (Aki & Richards 1980). These data, even when re-parameterized into x-p or tau-p, exhibit a response to a low-velocity zone that is a discontinuity or data gap which may be quite small even for a low-velocity zone that occupies a large crustal interval. The solution for a velocity–depth function requires integration across this gap. Traveltime inversion schemes often formally exclude low-velocity zones (Garmany 1979; Orcutt 1980; Diebold & Stoffa 1981) as a condition for developing an inversion algorithm, and although the inclusion of such features into the Herglotz–Bateman–Wiechert inversion has been demonstrated by Gerver & Markushevich (1966), it is seldom used because it is complex and difficult to develop into an efficient algorithm. Diebold (1988) has suggested a procedure for inclusion of low-velocity zones into the tau-sum inversion

* Also at Department of Geological Sciences, Columbia University, New York.

(Diebold & Stoffa 1981) in which a range of possible low-velocity zone properties are derived.

Spudich & Orcutt (1980a, b) summarized the results of several experiments from which it had been suggested that a low-velocity zone may be present in, or beneath, the oceanic crust. Most noteable is that of Lewis & Snydsman (1977, 1979) who presented a structural interpretation of the young oceanic crust of the Cocos Plate that included a low-velocity zone at the base of the crust that increased in thickness with age. We are aware of no similar suggestion for the crust of the Atlantic or any other slowly spreading ridge, although the data base is not very extensive.

In this study we examine high quality expanding spread profiles from the North Atlantic transect (NAT Study Group 1985) in an attempt to make a definitive statement about the existence of a low-velocity zone in the lower oceanic crust. These data are available at 50-m seismogram spacing, allowing for detailed analysis in the offset-travel time (x-t) and the intercept time-ray parameter (tau-p) domains. We were able to analyse tau-p seismograms with ray parameters sampled at 0.001 s km^{-1} increment even for the deepest arrivals. From a combination of x-t and tau-p analysis we present interpretations that, we believe, provide firm evidence for a low-velocity zone at ESP 5 (see Fig. 1 for location). Our preliminary interpretation of this low-velocity zone was presented by NAT Study Group (1985). Chiang & Detrick (1985) have modelled P- and S-wave arrival amplitudes in ESP 5 together with nearby CDP reflection profiles. They have also concluded that there is evidence for a crustal low-velocity zone. Huang, Chu & Kuo (1986) applied a waveform inversion method to plane-wave decomposed ESP 5 data, and supported the presence of a similar low-velocity zone. Cary & Chapman (1988) applied an automatic 1-D waveform inversion to ESP 5 data, and have concluded, to the contrary, that a low-velocity zone is not necessarily required to satisfy the data.

In this paper we describe the detailed analysis of ESP seismogram data that lead us to conclude that a low-velocity zone exists in 118 Myr old oceanic crust at ESP 5 in the N Atlantic. We then compare this result with solutions for crustal structure obtained from ESP data in both younger and older crust of the N Atlantic, and in doing so attempt to constrain the origin of the low-velocity zone.

DATA ACQUISITION AND ANALYSIS

The data analysed in this study were acquired as expanding spread profiles (ESPs). This method of seismic data acquisition was originally described by Stoffa & Buhl (1979) and has been extensively applied in deep crustal studies (see, for instance, Diebold *et al.* 1981; Mutter, Talwani & Stoffa 1984; Watts *et al.* 1985; NAT Study Group 1985; LASE Study Group 1986; Detrick *et al.* 1987; White *et al.* 1987; Diebold, Stoffa & LASE Study Group 1988; Mutter & Zehnder 1988). The basis of the experiment involves two vessels, one shooting and the other recording from a towed hydrophone array, as they move in opposite directions with equal speed, maintaining a common midpoint. The advantage of an ESP over conventional refraction data is that the effect of lateral geological variations and dip of the layers is minimized by the common midpoint geometry (Diebold & Stoffa 1981). Analysis of ESP data provides an accurate velocity structure that pertains to its midpoint, but represents an average over the range of the experiment. The seismic source used for the experiment consisted of a tuned airgun array on *S/V Prospekta* (Prakla Seismos), comprising 30 airguns having a total volume of 3300 cubic inches, operating at 2000 psi, and fired on a 60-s cycle. This array had a broad bandwidth of approximately 6–65 Hz. The recording ship, *RV Moore* (University of Texas at Austin) towed a 48-channel streamer with 70-m group interval. Each group consisted of 20 hydrophones at 1.605 m spacing, providing a total group length of 30.5 m. Both ships steamed at 5 knots (9 km hr^{-1} = 150 m min^{-1}) which resulted in a 300-m increment in the source-to-receiver offset for each shot. This acquisition technique provided a high density of seismograms—one about every 6 m. The seismograms were summed in 50-m bins (each bin containing about eight traces) after a linear moveout correction corresponding to a phase velocity of 8 km s^{-1} was applied. This summing provides a signal to random noise improvement by a factor of about 2.5.

Expanding spread profiles designated ESPs 2, 4, 5 and 11 from the North Atlantic transect (NAT Study Group 1985) were analysed for this study (Figs 1 and 2). ESP 5 was acquired at the location of magnetic anomaly M0, where the age of the crust is 118 Ma (Kent & Gradstein 1986). Two DSDP holes (417 and 418) are located near ESP 5 (Donnelly *et al.* 1979; Salisbury *et al.* 1986). The magnetic anomaly map of Schouten & Klitgord (1977) shows fracture zones spaced about 50 km apart in this area. ESP 2 was acquired within the magnetic quiet zone between anomaly M25 and the Blake Spur anomaly (Fig. 2). The age of the crust at ESP 2 is about 160 Ma. ESP 4 lies immediately landward of the Blake Spur magnetic anomaly, where the age of the crust is poorly constrained, but is probably 170 Ma. ESP 11 was acquired at the Mid-Atlantic Ridge.

Our procedure for deriving velocity–depth models from these data was as follows: transformation of the data to the tau-p domain as described by Stoffa *et al.* (1981), construction of a velocity–depth structure using the tau-sum inversion (Diebold & Stoffa 1981) to obtain a starting model, computation of traveltime curves in the $x - t$ domain and comparison with the observed data to improve the model, and then computation of WKBJ seismograms (Chapman 1978) and comparison with the data to improve the model further. ESP 5 data were further analysed because they contained well-developed converted shear wave arrivals. To obtain the shear wave velocity structure we assumed that the P- to S-wave conversion took place at the sediment/crust interface, retained the layer thicknesses of the P-wave velocity structure, and adjusted shear wave velocities until ray-traced arrivals showed a satisfactory fit to the $x - t$ and tau-p data. The P- and S-velocity functions for ESP 5 were further improved and attenuation quality factors (Q_p and Q_s) determined by computing reflectivity seismograms (see Fuchs & Muller 1971; Kennett 1974; Wenzel, Stoffa & Buhl 1982; and Muller 1985, among others) for some trial models to match the absolute amplitudes of the data. In the following we discuss our analysis of these data, then describe some aspects of their interpretation with respect to the geology of the Atlantic oceanic crust in this region.

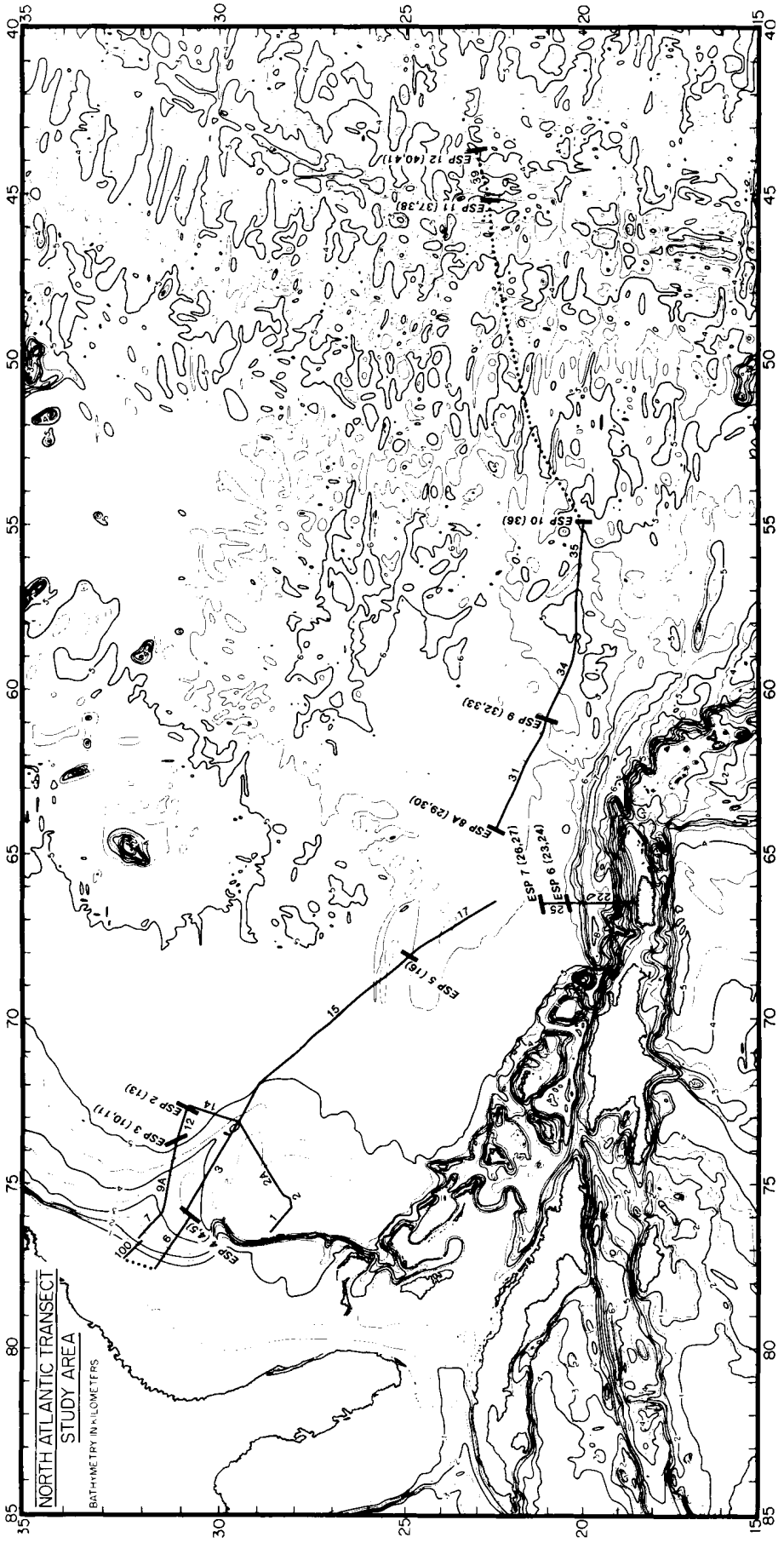

Figure 1. Location map of all expanding spread profiles (ESPs) acquired in the North Atlantic transect (NAT) experiment. Four ESPs (2, 4, 5 and 11) were used in this study. The numbers in parenthesis are the line numbers corresponding to the ESPs.

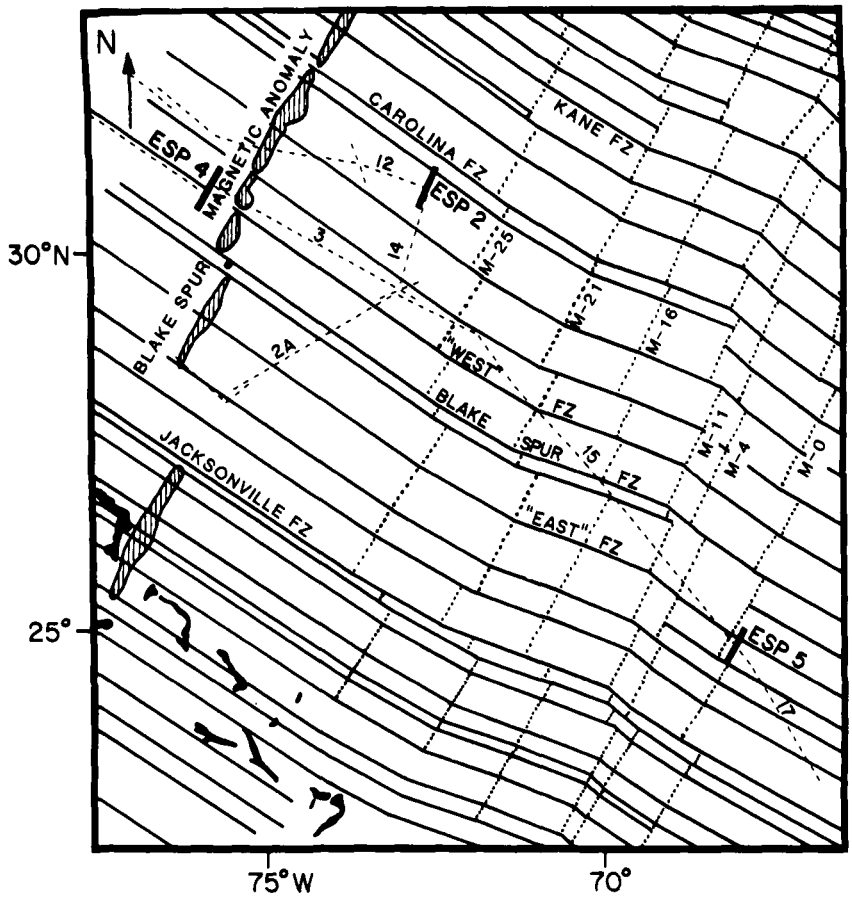

Figure 2. Location of ESPs 2, 4 and 5, superimposed on the map of Schouten & Klitgord (1977) showing the fracture zones based on magnetic lineations in the area of this study.

ANALYSIS OF NAT ESP 5

The ESP 5 seismogram data are shown in Fig. 3. Four groups of *P*-wave crustal arrivals have been identified. Group I and II arrivals are diving waves from the lower crust, group III arrivals are pre-critical reflections from Moho, and group IV arrivals are post-critical reflections and diving waves from the crust/mantle transition zone. The groups I and II arrivals are continuous. The division into two groups was made after initial trials at traveltime inversion for reasons that will be elaborated upon below. Group II arrivals terminate abruptly at a range of 32 km, suggesting the possible presence of a low-velocity zone.

The bathymetric observations at ESP 5 were available only from one ship (R/V *Moore*), so only half of the bathymetric profile has been shown (Fig. 4). The bathymetric profile, on a regional scale, can be approximated by an interface linearly dipping at an angle of 0° 20′. The common midpoint geometry of an ESP reduces the effect of this dip because the sum of the sea-floor depths below the source and the receiver remains approximately constant for a linearly dipping interface. This small dip is therefore not expected to affect adversely our overall traveltime analysis, and no topographic corrections were made. On a local level, however, this sea-floor bathymetry can affect the data—for example, the diving waves observed at approximately 14 km offset, 7.9 s reduced time (Fig. 3), are probably affected by some local sea-floor bathymetry. No attempt was made to correct for this local effect.

P-wave velocity (V_p) structure

Tau-sum inversion of these data was achieved in two steps. All data were transformed to the tau-p domain at a ray parameter spacing (dp) of 0.005 s km^{-1}. Using the post-critical arrivals in tau-p from $p = 0.667$ to 0.200 s km^{-1} the upper structure of *P*-wave velocities was derived. For the deeper part of the structure, derived from arrivals having ray parameters from 0.200 to 0.100 s km^{-1}, we found that a $dp = 0.005$ s km^{-1} was too coarse to use in the tau-sum inversion. The data from 20.0 to 37.5 km were slant-stacked at a dp of 0.001 s km^{-1}, from which the lower crustal and crust/mantle arrivals could be clearly resolved, as shown in Fig. 5 (upper panel). Also shown, in the lower panel of Fig. 5, are the tau-p picks. These picks represent only a part of the complete tau-p curve of principal arrivals, and therefore were used in conjunction with the upper structure derived earlier. For this purpose the tau-contribution of the 'known' upper structure was subtracted from the observed tau values before implementing tau-sum inversion at each ray parameter.

The velocity function obtained by this two-step tau-sum inversion is shown in Fig. 6 (left panel). The structure

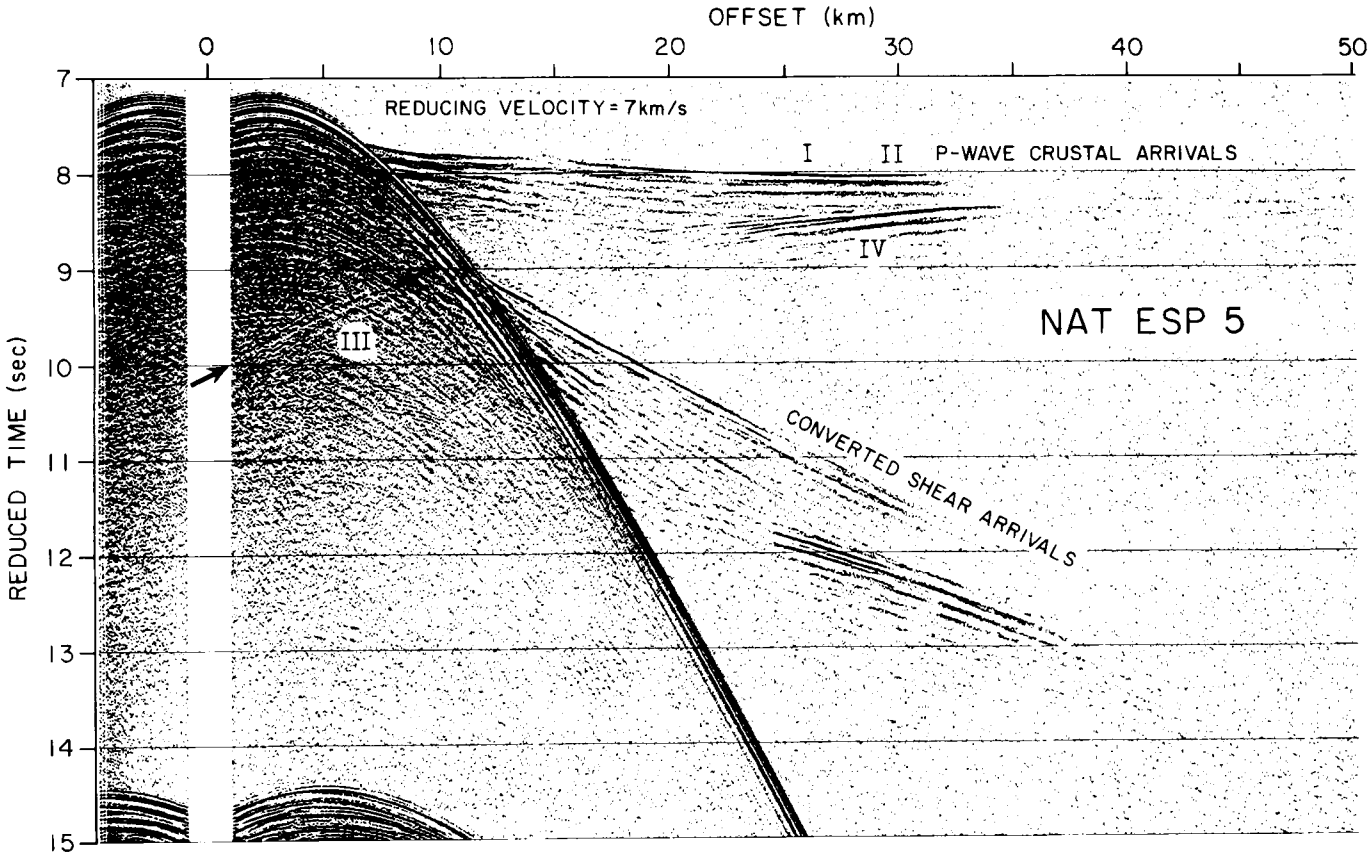

Figure 3. N Atlantic transect expanding spread profile 5 (NAT ESP 5). The data have been gathered in 50-m bins, summed, bandpass-filtered 6–40 hz, and plotted in true amplitudes with a reducing velocity of 7 km s^{-1}. Four groups of *P*-wave crustal arrivals and converted shear wave arrivals have been identified—see text for details.

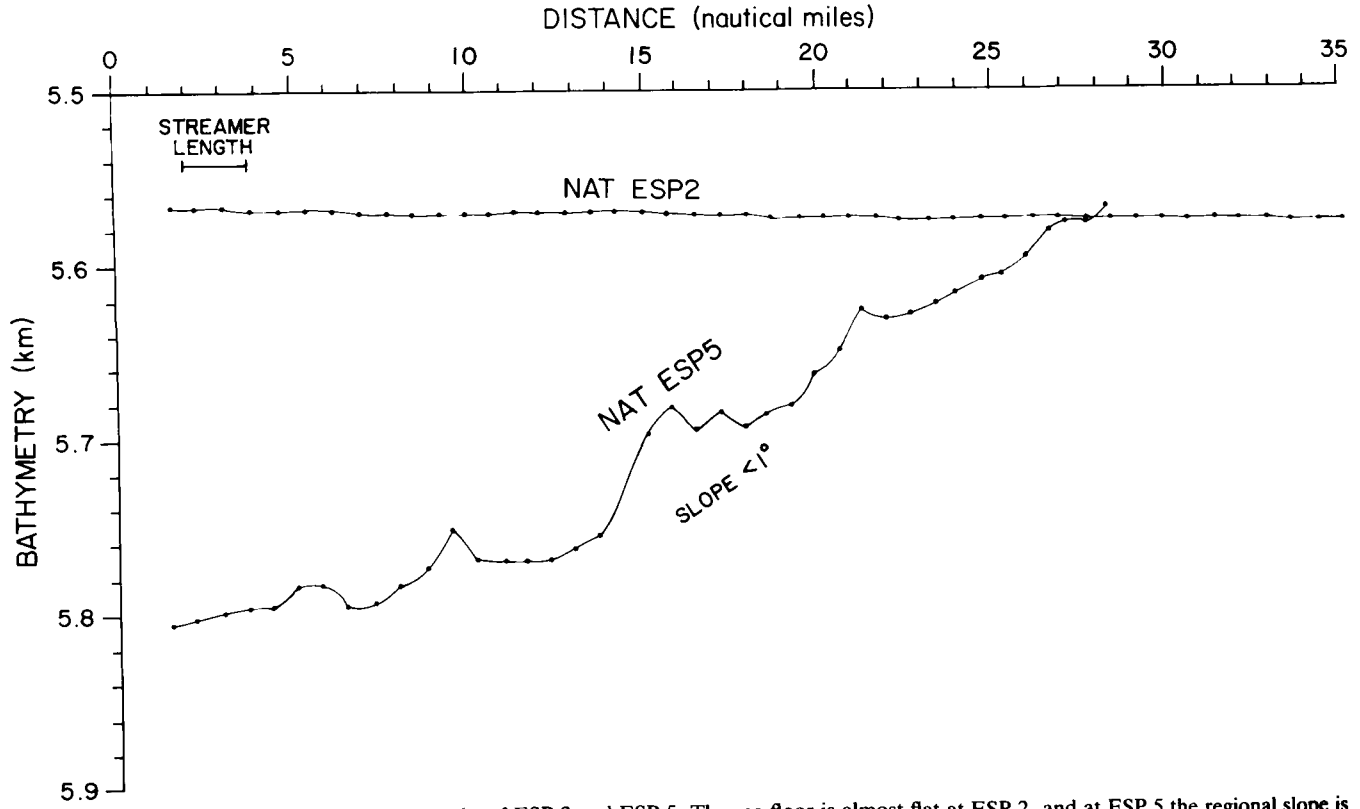

Figure 4. Bathymetry along the navigation tracks of ESP 2 and ESP 5. The sea floor is almost flat at ESP 2, and at ESP 5 the regional slope is 0°20′.

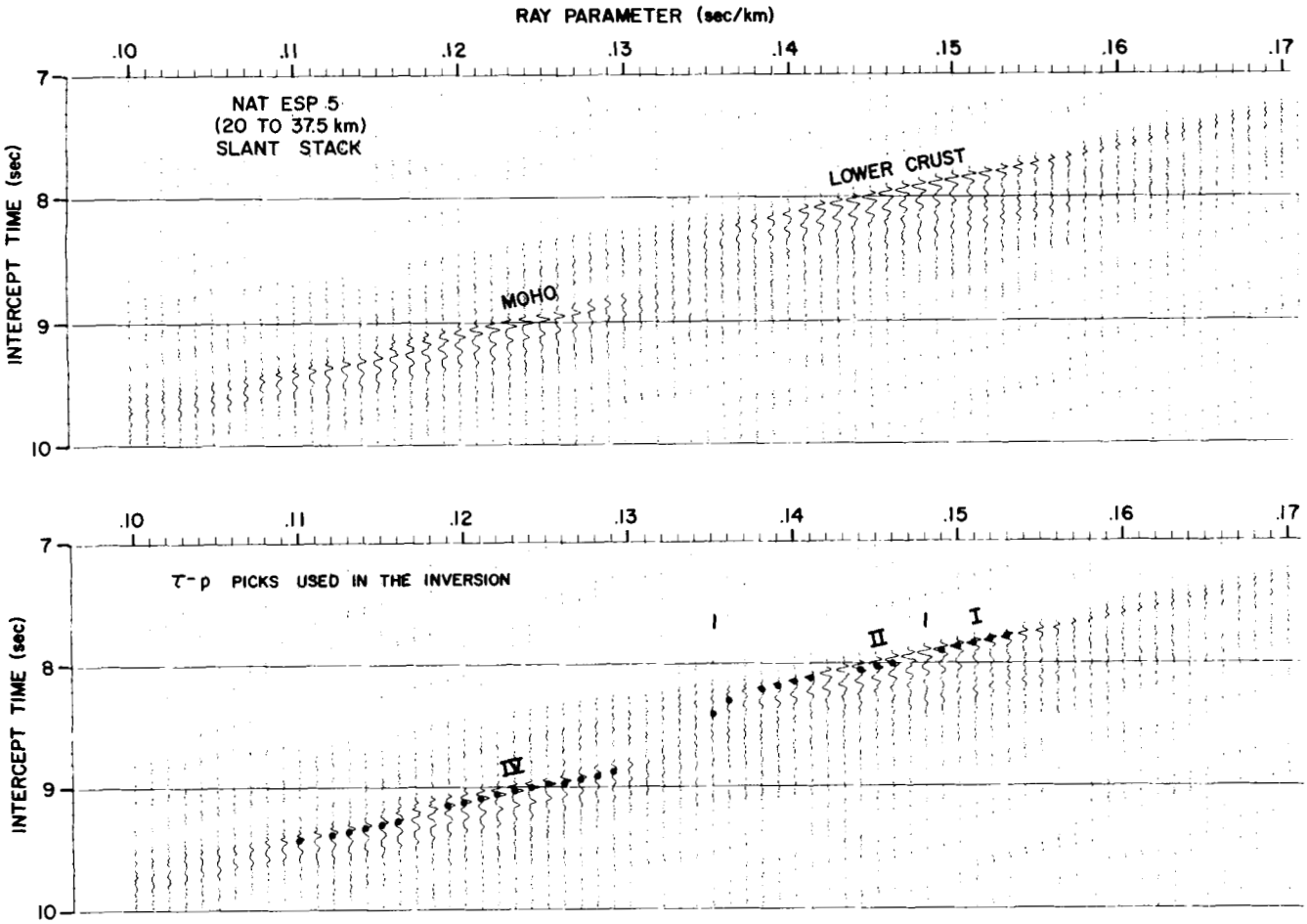

Figure 5. Slant stacks of ESP 5 data between 20 and 37.5 km offsets focus the lower crust and Moho *P*-wave arrivals. The tau-*p* picks obtained from the slant stacks are shown in the lower half of the figure. The groups of arrivals marked as I, II and IV correspond to similar groups in *x*-*t* shown in Fig. 3.

contains several layers having unphysical 'negative' thicknesses. Such layers can result from tau-sum inversion in two situations—one occurs if a pre-critical reflection is included in the inversion, and the other if a low-velocity zone is present in the real Earth structure. Considering the first of these we note that the tau-sum method derives layer thicknesses in an Earth approximated by a stack of uniform-velocity layers by a method that is essentially an extension of the classic slope–intercept method of Ewing, Woollard & Vine (1939), who used head-wave data. Diebold & Stoffa (1981) showed that it could be generalized to include diving waves and post-critical reflections. Vera & Diebold (1984) have discussed a further generalization of this approach in which the velocity function within each layer can be prescribed by a chosen analytic function, such as a linear gradient. If, however, pre-critical reflections are used in any form of the tau-sum inversion it will overestimate the thickness of the underlying layer. This overestimation is then compensated by reduction in the solution thickness of one or more layers defined from the post-critical arrivals of smaller ray parameter. The negative thickness layers, such as those around 15 km depth in Fig. 6 (left panel), can be corrected as shown in Fig. 6 (middle panel) if we ignore the arrivals from $0.135 < p < 0.148\ \mathrm{s\ km^{-1}}$ (Fig. 5), i.e. if we connect group I directly to group IV, treating group II arrivals as pre-criticals. Group II arrivals, however, seen clearly in $x-t$ (Fig. 3) are continuous with group I arrivals and have phase velocities that increase with increasing offset, and are therefore not pre-critical reflections. Thus, the negative thickness layers obtained in the inversion cannot be attributed to the inclusion of pre-critical reflections.

Group II arrivals can be retained and the negative thickness layers eliminated if we include a low-velocity zone in the structure (Fig. 6, right panel). Since a low-velocity zone does not produce post-critical arrivals, it cannot be included in the tau-sum inversion directly. An inversion can still be obtained for the region above the lid of the low-velocity zone, but to continue the inversion downwards we need to modify the method. For this purpose an algorithm was developed that proceeds in the following steps:

(1) Reads the upper structure obtained using a normal inversion.

(2) Accepts values for the velocity and thickness of the lid and the low-velocity zone.

(3) Redefines the tau-*p* points below the tau-gap with respect to the bottom of the low-velocity zone.

(4) Carries out the inversion below the low-velocity zone.

Using this approach different combinations for the lid and

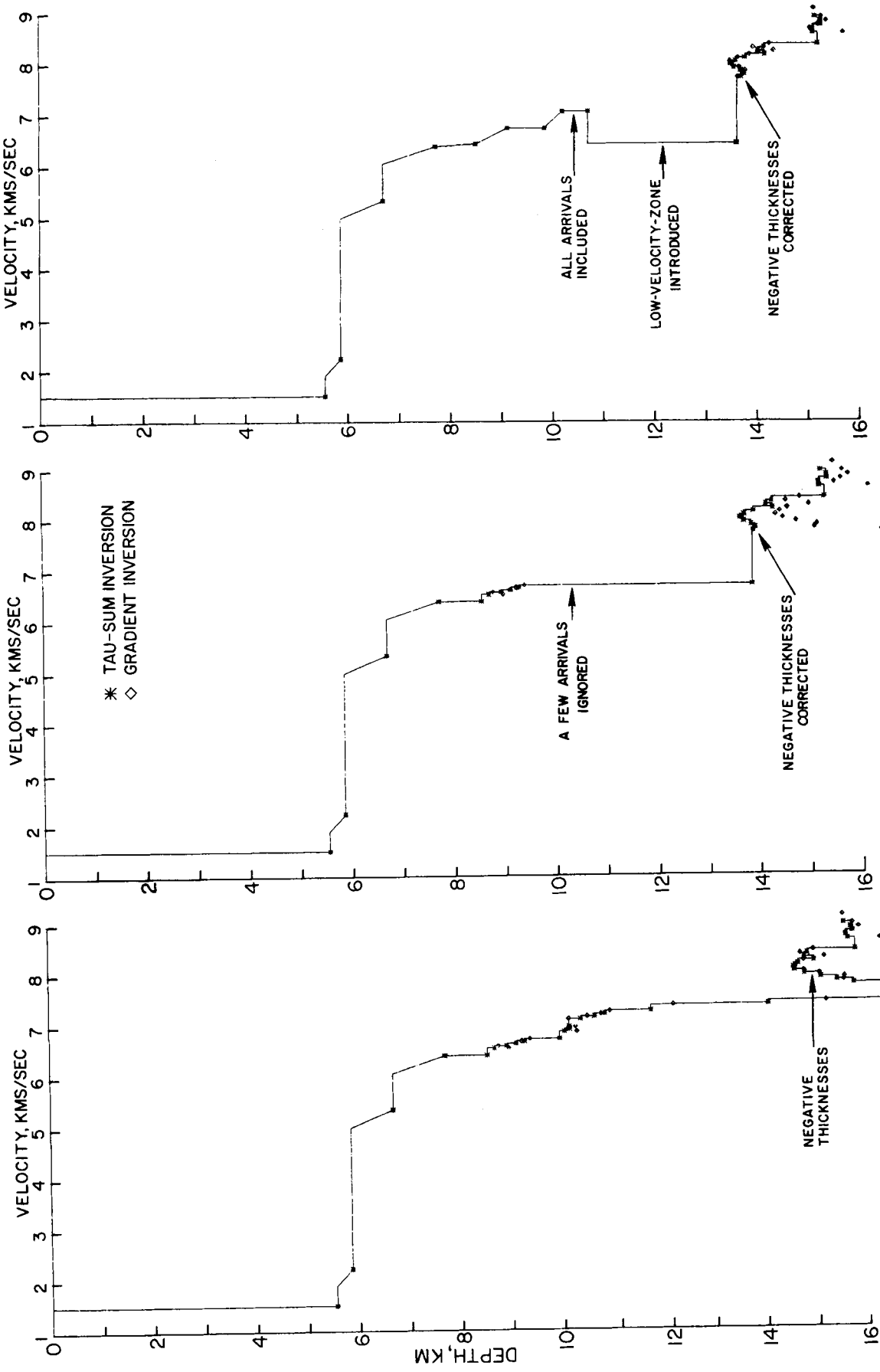

Figure 6. Left panel: velocity function obtained by tau-sum inversion using the tau-p picks shown in the lower panel of Fig. 5. The upper four layers in this structure were obtained separately. Centre panel: velocity function obtained by ignoring the group II arrivals (0.135–0.148 s km^{-1}). Right panel: velocity function obtained by providing structure down to 10.6 km after smoothing the function shown in left panel, introducing a low-velocity zone below that depth, and then using group IV arrivals (0.119–0.130 s km^{-1}). In all three panels, note that the tau-sum inversion points are connected by straight lines, whereas the gradient inversion points are not connected.

low-velocity zone were continuously tested and, based on the results obtained below the low-velocity zone, models were either discarded (if they gave negative thicknesses, for example), or taken as possible solutions.

In principle there are four independent variables that are undefined—the velocity of the lid, its thickness, the velocity of the low-velocity zone and its thickness. The data provide constraints that can be used to estimate one or more of these unknowns as follows:

(1) The *P*-wave velocity in the lid may be estimated from the bottom of the upper structure, i.e. from the slope of the most distant part of the diving waves from the crust ($7.14\,km\,s^{-1}$).

(2) The thickness of the lid may be estimated using near-vertical reflections from the bottom of the lid (not available in ESP 5).

(3) The total thickness of the lid plus the low-velocity zone may be estimated from the two-way time at which the tau-sum inversion stabilizes following the negative thickness layers (Mithal 1986).

(4) The total thickness of the lid plus the low-velocity zone may also be estimated from the near-vertical reflections from below the low-velocity zone.

We obtained upper structure down to a total depth of approximately 10 km by smoothing the velocity function shown in the left panel of Fig. 6. We then took the tau-picks shown in the lower panel of Fig. 5 and applied the method of inversion outlined above. The velocity function that we obtained is shown in the right panel of Fig. 6. Note that all observed arrivals were used and all negative thickness layers have been corrected. In all three panels of Fig. 6 the inversion results obtained by the 'gradient inversion' method (Vera & Diebold 1984) are also shown.

The *P*-wave velocity function obtained by using tau-sum inversion was improved by computing and comparing the traveltime curves with the data in the x-t domain. The improvements, however, were minor, and the major feature of the presence of a low-velocity zone was not affected. Our final *P*-wave velocity function is shown in Fig. 7 (model NE5B9, V_p) and given in Table 1.

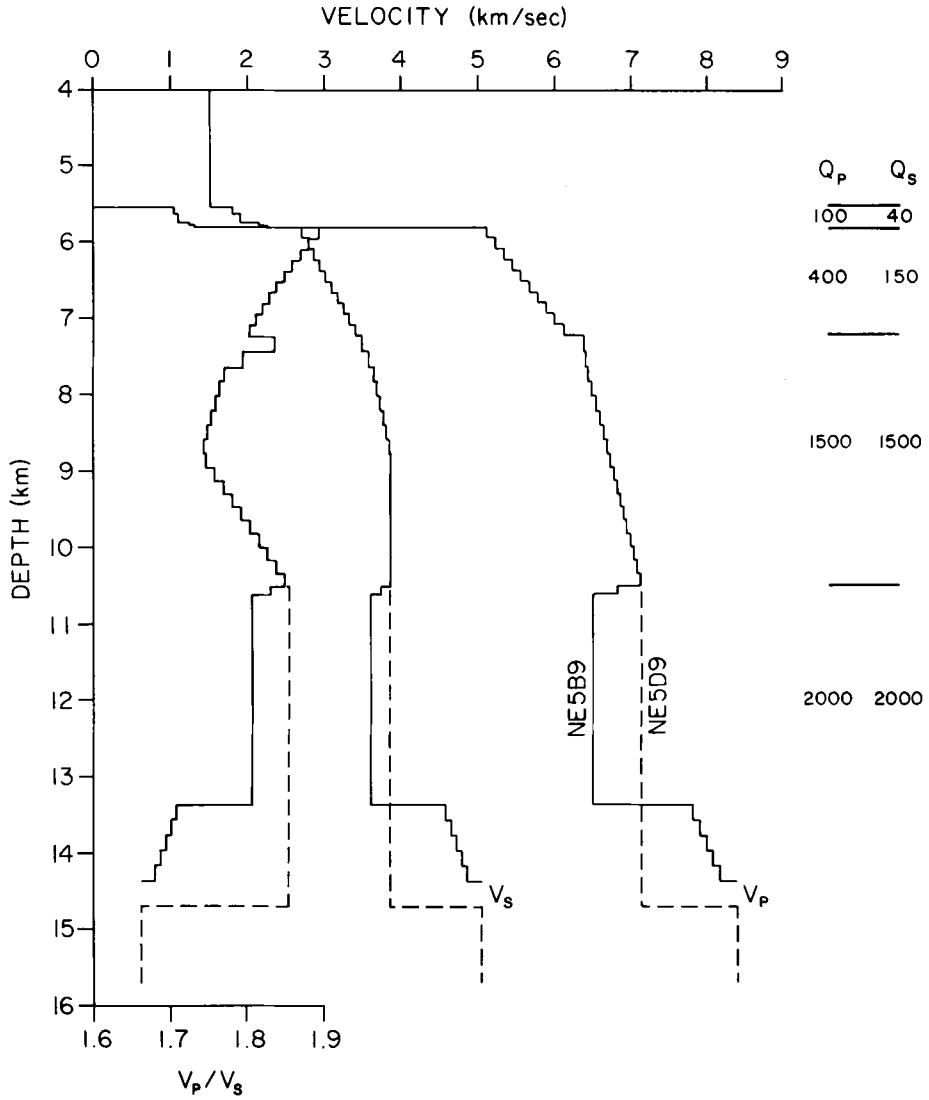

Figure 7. Model NE5B9 (shown by continuous lines) is our final model determined from the traveltime and amplitude analysis of NAT ESP 5 data. *P*-wave velocity (V_p), *S*-wave velocity (V_s), *P*-wave attenuation (Q_p), *S*-wave attenuation (Q_s) and V_p/V_s ratio are shown. Numerical values for this model are given in Table 1. Model NE5D9 (shown by dashed lines) was derived from the main model by eliminating the low-velocity zone and matching group IV arrival times. The reflectivity seismograms for these models are shown in Figs 8, 9 and 11.

Table 1.

Model NE5B9

LAYER		VPTOP (km/s)	VPBOT (km/s)	DZ (km)	VSTOP (km/s)	VSBOT (km/s)	QP	QS
1	water	1.510	1.510	5.565	0.0	0.0	0	0
2	Sediments	1.800	1.800	0.090	1.039	1.039	100	40
3	Sediments	1.900	1.900	0.102	1.097	1.097	100	40
4	Sediments	2.100	2.300	0.064	1.212	1.328	100	40
5	Upper Crust	5.050	6.160	1.415	2.660	3.425	400	150
6	Lower Crust	6.360	6.400	0.415	3.425	3.610	1500	1500
7	Lower Crust	6.400	6.700	1.135	3.610	3.850	1500	1500
8	Lower Crust	6.700	7.140	1.735	3.850	3.850	1500	1500
9	Lower Crust	7.140	6.500	0.100	3.850	3.600	2000	2000
10	Lower Crust	6.500	6.500	2.760	3.600	3.600	2000	2000
11	C/M Trans.	7.770	8.200	1.000	4.540	4.890	2000	2000
		8.400			5.050		2000	2000

S-wave velocity (V_s) structure

The *S*-wave velocities were determined using traveltime and amplitude data assuming that the *P*- to *S*-wave conversion occurred at the sediment/basement interface. While iterating to improve the *S*-wave velocity function, the *P*-wave velocities and the layer thicknesses were kept fixed. Our final *S*-wave velocity function is shown in Fig. 7 (model NE5B9, V_s) and given in Table 1.

Quality factors, Q_p and Q_s

The combined *P*- and *S*-wave velocities and densities were used to compute synthetic seismograms using the reflectivity method. Because the reflectivity method can deal only with constant-velocity layers, the gradients in the velocity model were simulated by several uniform-velocity layers. The layering associated with reflectivity need be no finer than one-half the shortest seismic wavelength (Chapman & Orcutt 1985). These seismograms were convolved with a source time function obtained from a near-vertical sea-floor reflection ($x = 1.85$ km) in ESP 5. This source wavelet is shown in Fig. 8 (lower panel, inset).

The densities were obtained from the *P*-wave velocities using the relationships,

$\rho\ (\mathrm{g\,cm^{-3}}) = 1.135\,V_p - 0.190,$

for $V_p \leq 2.0\ \mathrm{km\,s^{-1}}$ (Hamilton 1978),

$\rho\ (\mathrm{g\,cm^{-3}}) = 1.74\,(V_p)^{1/4},$

for $V_p > 2.0\ \mathrm{km\,s^{-1}}$ (Gardner, Gardner & Gregory 1974); density of water was taken to be 1.0.

The relative amplitudes of *P*-wave crustal arrivals in the synthetic seismograms for model NE5B9 were first computed without including attenuation (Fig. 8, middle panel). They compare reasonably well with the data (Fig. 8, upper panel) but the following problems remain: (1) the absolute amplitudes of *P*-wave crustal arrivals are approximately twice as high in synthetic seismograms as in the data, (2) the amplitude of *S*-wave crustal arrivals relative to the *P*-wave crustal arrivals is higher in synthetic seismograms than in the data, and (3) there are *S*-wave interbed multiples in model seismograms, but not in the data.

In an attempt to obtain a better match to the observed arrival amplitudes we used a trial and error approach by computing synthetic seismograms for a suite of Q_p and Q_s values in each layer. The Q values which reasonably explain the data are given in Table 1.

Two important features that emerged from this analysis are that Q_p for the uppermost crust is much smaller than for the lower crust, and that we need much higher values of Q_p in the lower crust than used by Spudich & Orcutt (1980a, b) in their detailed analysis of Fanfare data. Furthermore, in the lower crust our results show that $Q_s = Q_p$, *not* Q_s approximately one-half of Q_p, as is often assumed.

The synthetic seismograms for our final model NE5B9, which includes attenuation quality factors, are shown at 500-m spacing in Fig. 8 (lower panel), and at 50-m spacing in Fig. 9. A comparison of the synthetic seismograms with data (Fig. 8, upper panel, and Fig. 3 respectively) shows that by introducing these Q values not only the relative amplitudes but also the absolute amplitudes of *P*-wave crustal arrivals are matched. The amplitudes of *S*-wave crustal arrivals relative to the *P*-wave crustal arrivals have also improved, and the noise in the *S*-wave crustal arrivals due to the interbed multiples has been significantly reduced, matching better with the data.

Discussion of Model NE5B9 and some alternatives

Model NE5B9 (Fig. 7, Table 1) shows a crust that is 7.56 km thick. The details of the crust (layers 5–10, Table 1), and the crust/mantle transition (layer 11, Table 1) are given below:

0–1.415 km. *P*-wave velocities increase from 5.05 to 6.16 $\mathrm{km\,s^{-1}}$, and the *S*-wave velocities from 2.66 to 3.42 $\mathrm{km\,s^{-1}}$ resulting in a Poisson ratio [$\sigma = [(r^2 - 2)/2(r^2 - 1)]$, where $r = V_p/V_s$] decrease from 0.31 to 0.28.

1.415–1.830 km. In this interval the *P*-wave velocities (6.36–6.40) do not maintain the velocity gradient of the overlying layer while the *S*-wave velocity gradient (3.42–3.61 $\mathrm{km\,s^{-1}}$) is maintained. The Poisson ratio decreases further (0.30 to 0.27).

1.830–2.964 km. *P*-wave velocities (6.40–6.70 $\mathrm{km\,s^{-1}}$) as well as the *S*-wave velocities (3.61–3.85 $\mathrm{km\,s^{-1}}$) have a less steep gradient than in the uppermost layer of the crust. The Poisson ratio continues to decrease (0.27 to 0.25).

2.965–4.700 km. *P*-wave velocities (6.70–7.14 $\mathrm{km\,s^{-1}}$) continue to increase with the same gradient as in the overlying

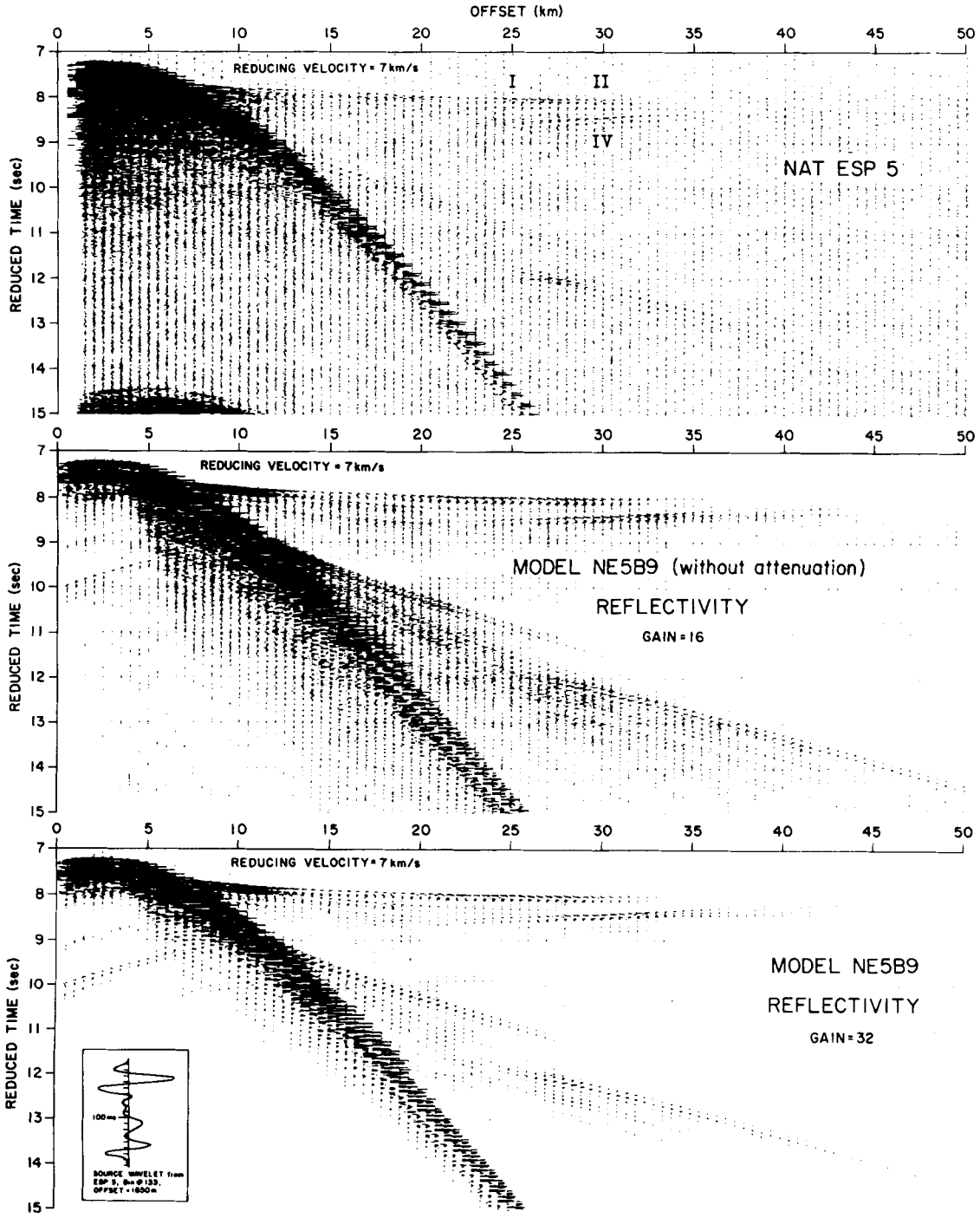

Figure 8. Upper panel: NAT ESP 5 data shown at 500-m spacing. The amplitudes and waveforms of the *P*-wave crustal arrivals (groups I, II and IV), and the converted shear arrivals (see Fig. 3) can now be seen better because there is no clipping of the amplitudes. However, group III arrivals are seen better at 50-m spacing (in Fig. 3). Middle panel: synthetic seismograms for a model which has the same *P*-wave velocities, *S*-wave velocities and densities as in our final model (NE5B9), but which has no *P*- and *S*-wave attenuation. These seismograms were computed using the reflectivity method, and convolved with the source time function obtained from a near-vertical sea-floor reflection in the data. The arrival times and amplitudes of *P*-wave crustal arrivals (groups I, II and IV, Fig. 3) match quite well with the data, and also the arrival times of converted shear waves are correct. However, the amplitudes of near-vertical sea-floor reflections in the synthetics are half of those in the data, the amplitudes of converted shear wave arrivals are higher, and there are a lot more reverberations, particularly of the converted *S*-waves. Lower panel: synthetic seismograms for our final model (NE5B9, Fig. 7) computed using the reflectivity method, and convolved with the source time function (shown in the inset). The arrival times and amplitudes of not only the *P*-wave crustal arrivals, but also of the near-vertical sea-floor reflections and of the converted shear arrivals now match those in the data.

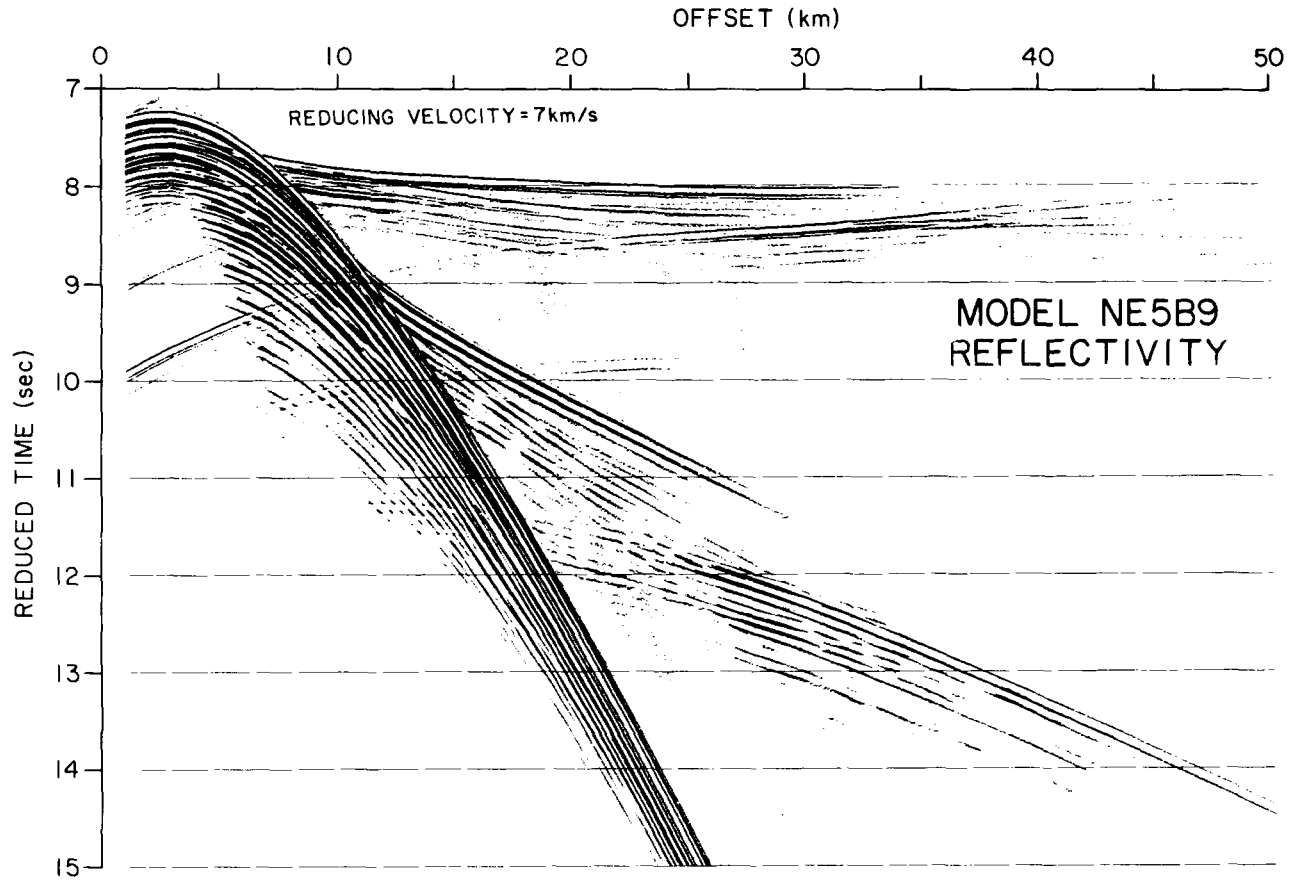

Figure 9. Synthetic seismograms at 50-m spacing for our final model (NE5B9, Fig. 7) computed using the reflectivity method and convolved with the source described in Fig. 8. These seismograms can be compared to NAT ESP 5 data shown in Fig. 3. Notice that not only groups I, II and IV, but also group III and the converted *S*-wave arrivals in the data compare well with the model.

layer, but the *S*-wave velocity is constant (3.85 km s^{-1}). The Poisson ratio begins to increase (0.25 to 0.30) at this level.

4.700–4.800 km. A 0.1-km-thick layer representing transition from velocities increasing with depth to the low-velocity zone.

4.800–7.560 km. This layer defines a 2.86-km-thick low-velocity zone which has a *P*-wave velocity of 6.5 km s^{-1} and an *S*-wave velocity of 3.6 km s^{-1}. The Poisson ratio (0.28) is the average of the ratio in the layer immediately overlying it. In the uppermost 100 m the *P*-wave velocity decreases from that in the lid (7.14 km s^{-1}) down to the velocity in the low-velocity zone (6.5 km s^{-1}).

7.560–8.560 km. A 1.0-km-thick layer representing a transition zone characterized by *P*-wave velocities from 7.77 to 8.20 km s^{-1}, and *S*-wave velocities from 4.54 to 4.89 km s^{-1}. The mantle beneath this transition zone has a small velocity increase ($V_p = 8.4$ km s^{-1}, $V_s = 5.05$ km s^{-1}).

One of the most interesting features of the velocity model we propose is the low-velocity zone in the interval 4.7–7.56 km. No previous study of slow-spreading oceanic crust has revealed such a feature and thus we believe it is important to substantiate our proposed model as carefully as possible and investigate some plausible alternative structures. In fact some features of the ESP 5 seismograms are not completely explained by the low-velocity zone model. The diving *P*-waves from the upper crust have two amplitude minima—one at approximately 14.5 km offset and 7.9 s reduced time; the other at approximately 22 km offset and 8.0 s reduced time (Fig. 3)—and these are not seen in the synthetic seismograms. Group IV arrival times and amplitudes are correctly modelled but some aspects of the waveforms are not—for example at approximately 30 km offset and 8.5 s reduced time the model correctly predicts the amplitude maximum, but the model waveforms are not correct (Fig. 8). Further, there are two branches merging into branch at approximately 28 km offset and 8.5 s reduced time (Fig. 3) which cannot be explained very well by this model (Fig. 9). For the *S*-wave Moho arrivals there are also two branches which are more or less parallel (Fig. 3, approximately 25–30 km offsets and 12 s reduced time)—this feature in the data also cannot be explained well by model NE5B9.

To improve confidence in the low-velocity zone model NE5B9 we considered several models without a low-velocity zone (Fig. 10). If the low-velocity is replaced by a layer having the same velocity as that above we cannot simultaneously match the pre-critical and the post-critical reflections from Moho. If we match the pre-critical arrival times, the post-criticals in the model occur too early (Model NE5C9, Fig. 10, upper panel). Increasing the thickness of this layer allows us to satisfy post-critical reflection time but the pre-criticals appear too late (Model NE5D9, Fig. 10, middle panel). This is a model likely to be obtained if

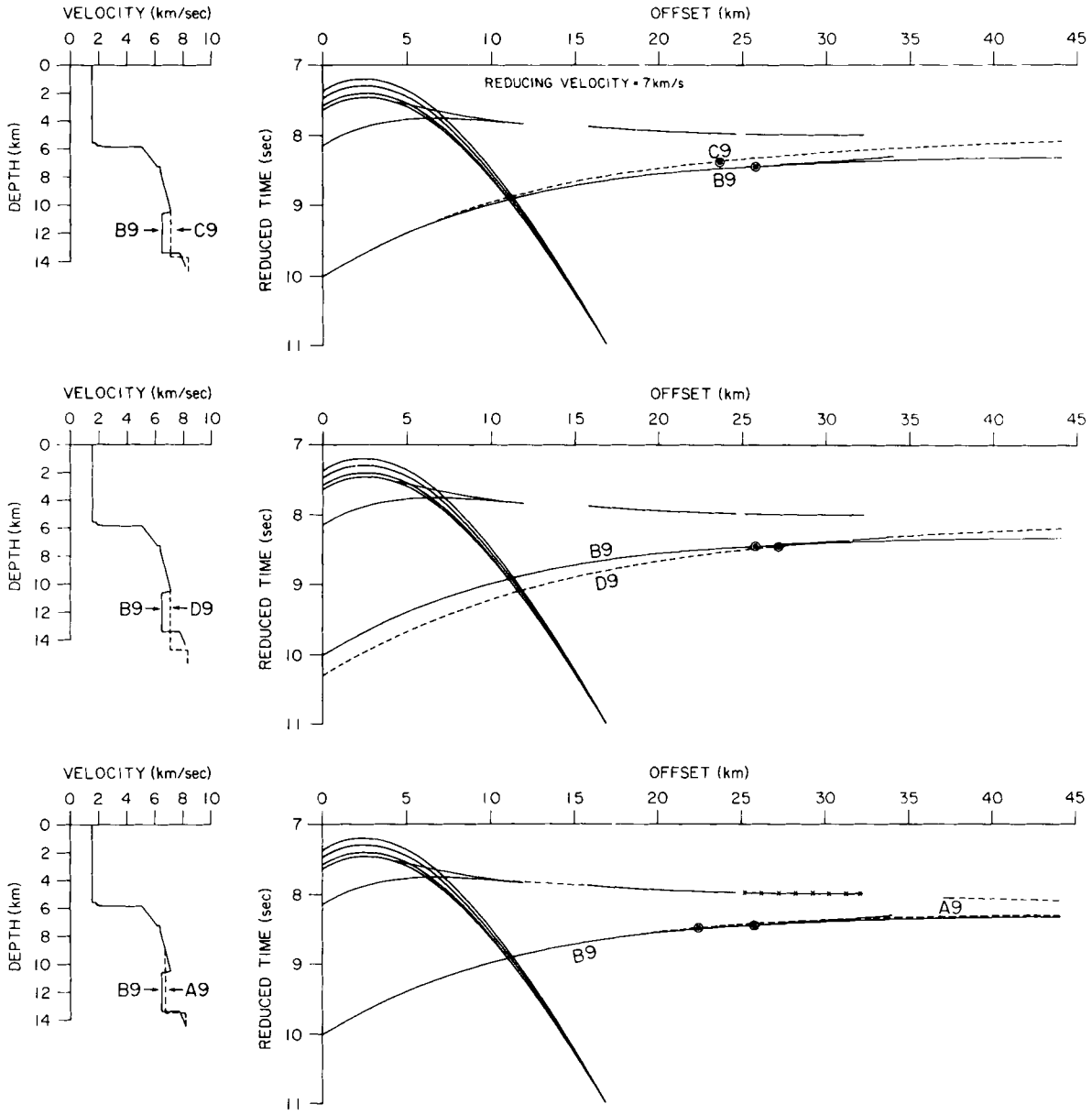

Figure 10. Comparison of traveltime curves for three models without low-velocity zone, with the curves for our final model (NE5B9). A continuous line with crosses represents that part of the curve which exists for NE5B9, but not for the model being compared.

pre-critical reflections from Moho (group III) are not properly considered. To achieve a simultaneous fit without a low-velocity zone we are required to alter the structure above this layer (Model NE5A9, Fig. 10, lower panel). This model does not produce the first arrivals between 25 and 32 km offsets (shown by continuous line with crosses) seen in the data, and therefore is also unsatisfactory. *P*-wave velocities of our final model (NE5B9) and the corresponding traveltime curves are shown by heavy lines in all three panels for comparison with the three trial models that do not include a low-velocity zone.

Synthetic seismograms for model NE5D9 (Fig. 7) computed using the reflectivity method are shown in Fig. 11. Their comparison with the data (Fig. 8, upper panel) shows not only that the group III arrival times do not match, but also that group II arrivals do not fade out beyond approximately 32 km offset as abruptly as with the low-velocity zone model, and also the converted shear wave arrivals reflected from Moho are delayed and too weak.

ANALYSIS OF NAT ESPs 2, 4 AND 11

Identification of a low-velocity zone at the base of crust at the location of ESP 5 invites the question—how widespread is this feature? To address this question, we analysed three other ESP seismograms: ESPs 2 and 4 acquired in much older crust, and ESP 11 acquired in much younger crust (see Figs 1 and 2 for locations). *P*-wave velocity structure was derived from these ESPs by traveltime inversion in a fashion similar to that outlined above: tau-sum inversion to obtain a starting velocity–depth model, computation of traveltime curves in the $x-t$ domain and comparison with the

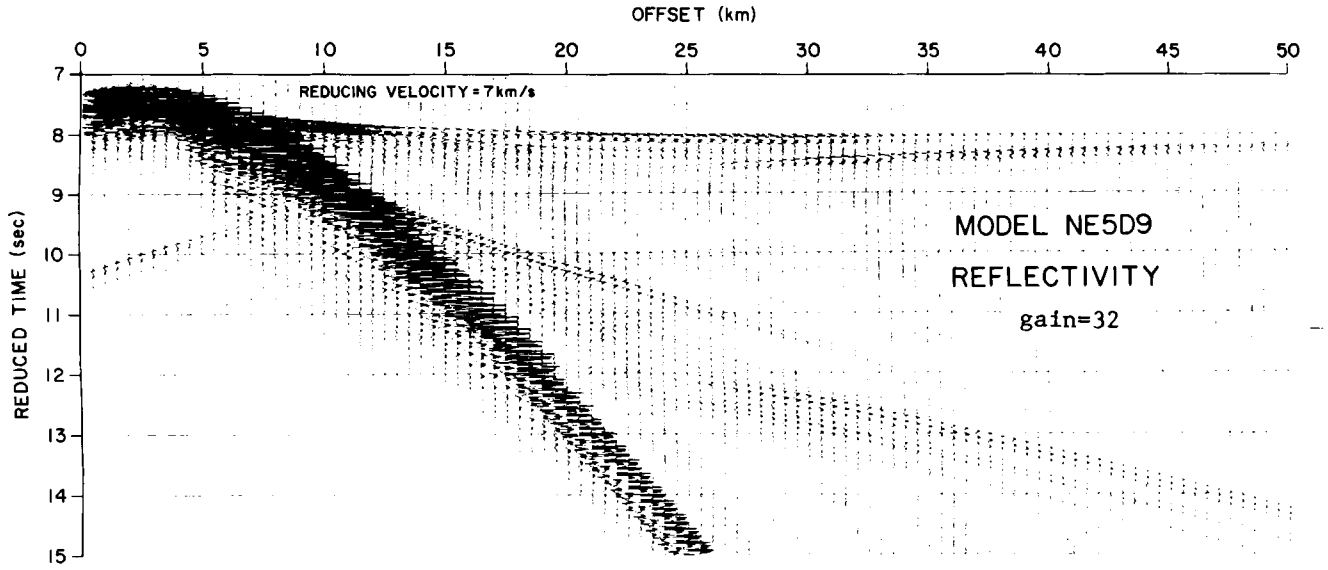

Figure 11. Synthetic seismograms for one model without a low-velocity zone (Model NE5D9, Fig. 7) computed using the reflectivity method. This is a model likely to be derived if group III arrivals are not included in the analysis. Comparing these seismograms with the data (Fig. 3 and upper panel of Fig. 8) show that the group III arrivals in the model are too late, and the converted shear wave arrivals reflected from Moho are also too late and too weak.

observed data to improve the model, and then computation of WKBJ seismograms and comparison with the data to improve the model further. *S*-wave velocities and densities were obtained from the *P*-wave velocities, and attenuation constants were not modelled.

The bathymetric profile at ESP 2 is very flat (Fig. 4) and therefore no topographic correction is needed. ESP 2 data and the WKBJ seismograms for our final model (NE2A, Fig. 16, Table 2) are shown in Fig. 12. In the data, the *P*-wave arrivals corresponding to groups I, II, III and IV of ESP 5 (Fig. 3) can be identified, but the time delay between groups II and IV in ESP 2 is much less than in the equivalent region of ESP 5. A comparison of these data and the WKBJ seismograms for model NE2A, which does not contain a low-velocity zone, shows not only that the traveltimes match well, but also that the relative amplitudes are in good agreement. Since attenuation constants have not been derived or applied, the absolute amplitudes are not correct. The phases marked 'T' in the WKBJ seismograms are artifacts due to the truncation of ray parameters (truncation phases).

ESP 4 was located immediately west of the Blake Spur magnetic anomaly. The bathymetry at ESP 4 was not recorded, but the regional bathymetry in this area is quite flat (Fig. 1). These data, shown in the upper panel of Fig. 13, are of lesser quality than ESP 5 or ESP 2. In particular, the arrivals equivalent to groups I and II of ESP 5 are not well developed and thus it is difficult to make an unequivocal assessment of the lower crust. However, the *P*-wave velocity structure that we have derived (model NE4A, Fig. 16, Table 2) does not include a low-velocity zone in the crustal section. A comparison of these data with the WKBJ seismograms (Fig. 13) shows that the overall arrival time match is good, and that high-amplitude events due to the wide-angle Moho reflections are in the correct offset range.

ESP 11 was acquired over the zero age Mid-Atlantic Ridge median valley (see Fig. 1 for location). Here the topography is very rough and this adversely affects seismic data; considerable energy is lost as diffractions, and the

Table 2.

	Model NE2A			Model NE4A			Model NE11A		
LAYER	VPTOP (km/s)	VPBOT (km/s)	DZ (km)	VPTOP (km/s)	VPBOT (km/s)	DZ (km)	VPTOP (km/s)	VPBOT (km/s)	DZ (km)
1	1.500	1.500	5.325	1.500	1.500	3.675	1.500	1.500	3.600
2	1.700	1.700	0.106	1.600	1.800	0.340	1.600	1.600	0.240
3	1.800	1.800	0.113	1.825	2.100	0.637	1.800	2.750	0.280
4	1.900	1.900	0.142	2.150	2.150	0.323	5.000	5.700	0.534
5	2.000	2.000	0.350	2.200	3.000	1.354	5.850	6.500	2.622
6	2.100	2.100	0.289	4.050	4.050	0.304	6.500	6.500	1.300
7	2.400	2.900	0.694	3.250	3.250	0.894	6.950		
8	4.928	6.700	2.856	3.900	5.000	0.443			
9	6.700	6.800	0.776	5.000	6.300	0.619			
10	6.800	7.050	1.835	6.300	6.800	1.408			
11	7.050	7.050	2.291	6.800	6.900	4.966			
12	7.650	8.000	1.369	7.150	8.050	2.277			
13	8.100			8.250	8.250	0.825			
				8.300					

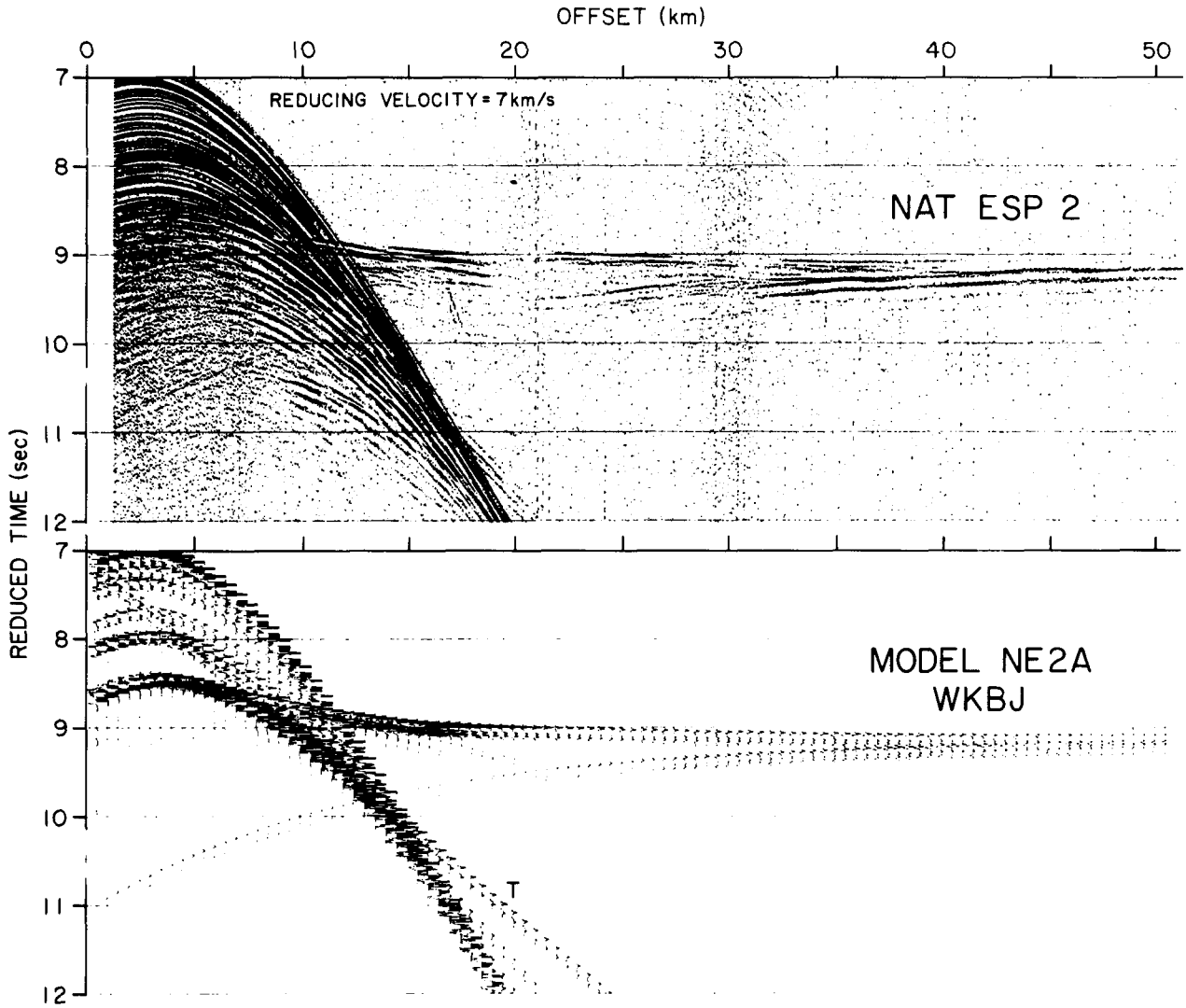

Figure 12. N Atlantic transect expanding spread profile 2 (NAT ESP 2) data shown in true amplitudes (for the location see Figs 1 and 2). Also shown are synthetic seismograms using the WKBJ method for our final model for this ESP (Model NE2A, Fig. 16, Table 2). The phases marked 'T' are artifacts due to the truncation of ray parameters.

arrival times of reflections and refractions depart from theoretical curves that are computed on a plane layer assumption. In ESP 11 (Fig. 14) fewer crustal reflections can be identified compared to other ESPs. In the velocity function obtained for ESP 11 (model NE11A, Fig. 16, Table 2), the highest *P*-wave velocity obtained is 7 km s^{-1} at about 8.5 km depth. Deeper crustal structure could not be obtained because of a lack of the corresponding arrivals. A comparison of the data with the WKBJ seismograms (Fig. 14) shows that the identifiable arrivals have been matched by our model NE11A. Since the deeper crustal structure could not be obtained from ESP 11, we cannot determine if a low-velocity zone exists within the lower crust at this location.

DISCUSSION

Low-velocity zone within the lower oceanic crust at NAT ESP 5

Our results from NAT ESP 5 show that a low-velocity zone occurs at the base of the oceanic crust at this location and, as such, is the first well-documented example of a low-velocity zone in Mesozoic aged crust in the Atlantic. Spudich & Orcutt (1980a) cite several studies from which the presence of crustal low-velocity zones in both compressional (*P*) and shear (*S*) wave velocities has been suggested. For instance, Lewis & Snydsman (1977, 1979) reported a V_p low-velocity zone at the base of oceanic crust in the northern Cocos plate based on an observed delay time offset between the wide-angle arrivals from the lower part of the crust and from the upper mantle, much like the evidence that we present here. The crust there varies in age from 2 to 12 Ma. Lewis & Snydsman (1977, 1979) suggested that the velocity in the low-velocity zone must be less than 6.8 km s^{-1} with a thickness of about 1.5 km, and interpret the low-velocity zone as the result of progressive serpentinization of upper mantle material into a material with 'crustal' velocities. Their low-velocity zone is therefore not strictly part of the original crust, but is 'added on' beneath through serpentinization. This process requires efficient, long-term transport of water into the upper mantle.

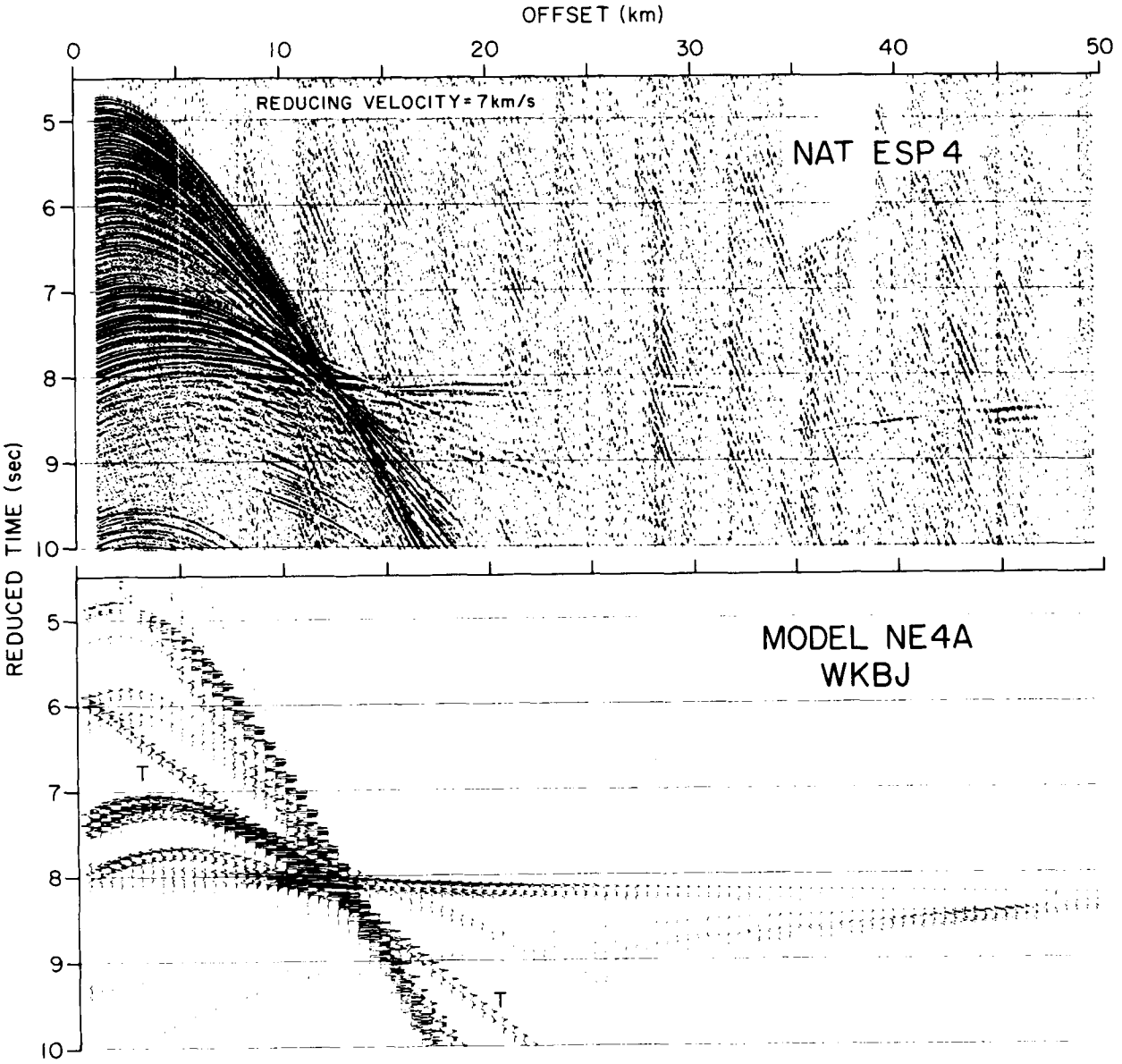

Figure 13. N Atlantic transect expanding spread profile 4 (NAT ESP 4) data shown in true amplitudes (for the location see Figs 1 and 2). Also shown are synthetic seismograms using the WKBJ method for our final model for this ESP (Model NE4A, Fig. 16, Table 2). The phases marked 'T' are artifacts due to the truncation of ray parameters.

Spudich & Orcutt (1980b) cite several studies that support the serpentinization interpretation based on evidence from ophiolite suites where serpentinized peridotite occurs beneath gabbroic units (for example, Clague & Straley 1977; Nichols *et al.* 1980). They also describe evidence for a low-velocity zone in V_s extending through most of the lower oceanic crust near Guadalupe Island, Mexico, from original work of Spudich, Salisbury & Orcutt (1978). Their evidence is also a delay time offset in lower crustal arrivals. In this latter case however they attribute the V_s low-velocity zone to the possible replacement of hornblende by augite and olivine with increasing depth into the lower oceanic crust at that site, and not to a mantle alteration phenomenon. The two explanations are, in fact, quite different in their implications for crustal geology; the mantle serpentinization model supposes that the low-velocity interval is not part of the crust's original igneous stratigraphy, but is incorporated into the crust by transformation of mantle into serpentinites by the action of deeply penetrating water. By contrast, the suggestion that the low velocities result from hornblende replacement considers the low-velocity zone to occur within the crust proper. Estimates of magma budget required to build the crust at ESP 5 would therefore differ by 50% depending upon which of these models one chose to adopt.

We believe that evidence provided by our analysis of ESP 5 favours an interpretation of the low-velocity zone as an integral component of the oceanic crustal column, rather than serpentenized mantle. Christensen & Salisbury (1975) show V_p, V_s and Poisson's ratio as a function of mineralogy for pure and isotropic monomineralic aggregates

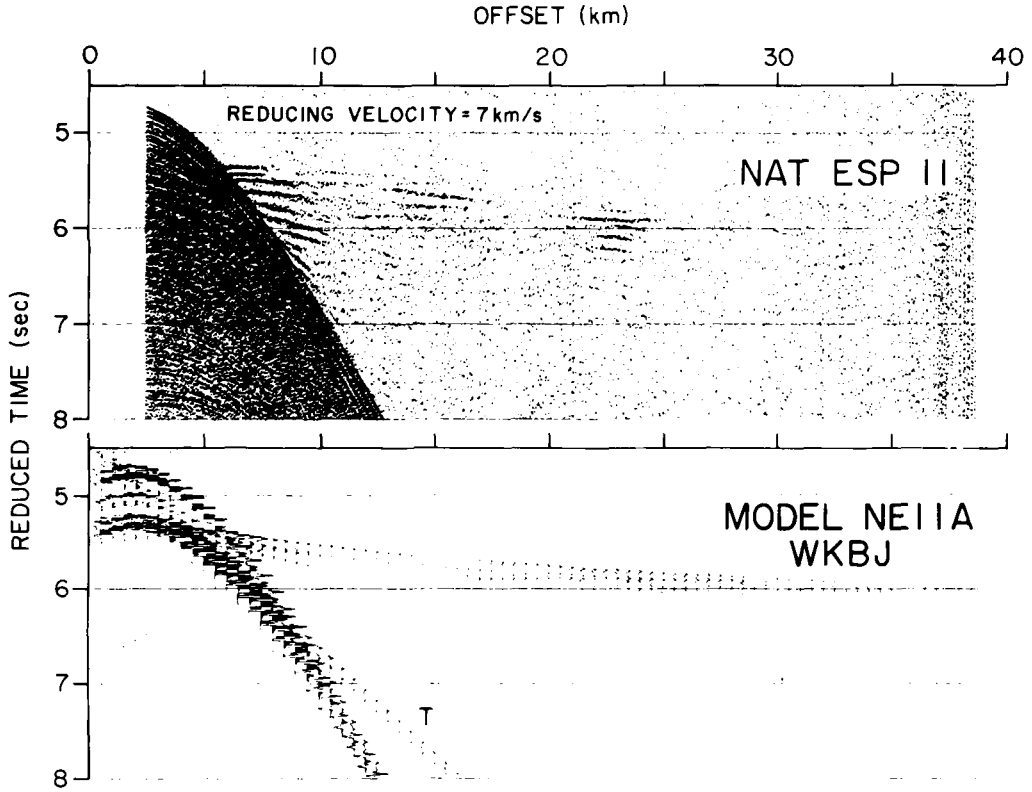

Figure 14. N Atlantic transect expanding spread profile 11 (NAT ESP 11) data shown in true amplitudes (for the location see Fig. 1). Also shown are synthetic seismograms using the WKBJ method for our final model for this ESP (Model NE11A, Fig. 16, Table 2). The phases marked 'T' are artifacts due to the truncation of ray parameters.

believed to represent two possible lithologies for the lower oceanic crust—a gabbro/metagabbro system and a peridotite/serpentinite system. A comparison with those observations indicate that the V_p and V_s values for the low-velocity zone at ESP 5 are consistent with about 40% serpentinization of a peridotite/serpentinite rather than gabbro/metagabbro lithology. However, laboratory measurements of V_p and V_s for the Bay of Islands ophiolite complex in Newfoundland (Salisbury 1974; Salisbury & Christensen 1978), for various western US ophiolites (Christensen 1978), and for the Oman ophiolite complex (Christensen & Smewing 1981) reveal that the V_p and V_s values of the low-velocity zone at ESP 5 *are* consistent with the more recent figures for metagabbros. Fig. 15 shows our low-velocity zone model NE5B9 on the laboratory velocity data compiled by Spudich & Orcutt (1980a) from the measurements of Salisbury (1974) and Christensen (1978). The low-velocity zone, shown by a 'star', is surrounded by metagabbro and metadolarite samples, and the remainder of the crust falls within or very close to the experimentally measured values. No part of the crust appears anomalous.

Another constraint on the nature of the low-velocity zone can be gained by comparison with other N Atlantic crustal velocity models. Fig. 16 shows that the total thickness of the crust at ESP5, including the low-velocity zone, is very similar to the crustal thickness at ESPs 2 and 4, both of which do not contain crustal low-velocity zone. Other determinations of crustal thicknesses in N Atlantic obtained earlier by Purdy (1983), White (1979, 1984), Whitmarsh, Ginsburg & Searl (1982), and Mutter & Zehnder (1988) are also shown in Fig. 16. These observations show that the low-velocity zone at ESP 5 definitely occurs within a depth interval in the crust that is normally regarded as oceanic layer 3, the gabbroic sequence (see for instance Fox & Stroup 1981). If mantle serpentinization was responsible for the development of the low-velocity zone we would anticipate that the crust containing the low-velocity zone would be thicker than that without, having acquired the low-velocity zone as an additional layer formed by serpentinization of mantle material that originally occurred beneath the normal crust. A thickening of the crust with crustal age is, in fact, the observation on which Lewis & Snydsman (1977, 1979) make their argument for a serpentinization model of the low-velocity zone. Because we observe a very similar crustal thickness in crust both with and without the low-velocity zone, we suggest that this argues against a regional serpentinization mechanism for the development of the low-velocity zone at NAT ESP 5. Therefore, we favour a crustal origin for the low-velocity zone, and believe that it is most likely to have a metagabbroic composition.

It is plausible that serpentinization could have locally affected structure at ESP 5. The shooting line extends into the region of the 'east fracture zone of Mutter & NAT Study Group (1985), however no offset in magnetic anomalies is seen at this location (Fig. 2), and McCarthy *et al.* (1988) recognized little structure in the migrated reflection seismic images associated with this feature. Nevertheless, local

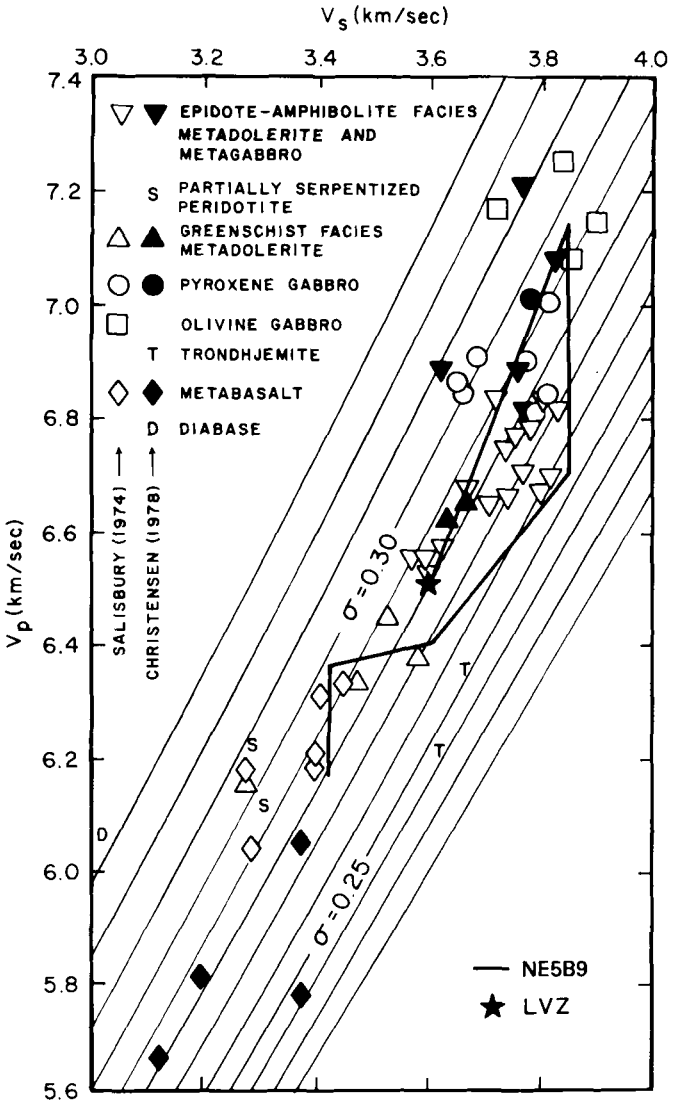

Figure 15. The V_p–V_s path for ESP 5, model NE5B9 compared with ophiolite sample velocities. The point shown by a 'star' corresponds to the low-velocity zone in the model.

serpentinization beneath an initially thin crust could account for the observed structure.

Crust/mantle transition

Because of the presence of both the pre-critical (group III) and the post-critical (group IV) reflections from Moho observed in ESP 5, we have been able to determine a well-constrained structure of the crust/mantle transition zone. It consists of a 1.0-km-thick velocity gradient (from 7.77 to 8.2 km s^{-1}), bounded by a major velocity discontinuity on top (6.50 to 7.77 km s^{-1}) and a minor velocity discontinuity at its bottom (8.20 to 8.40 km s^{-1}). The upper velocity discontinuity is constrained by the arrival times of group III and IV arrivals and the critical offset as inferred from group IV arrivals. The velocity gradient is constrained by the concentration of group IV arrivals whose amplitudes decrease abruptly rather than gradually with offset. The lower velocity discontinuity is not as well constrained.

The transition zone determined from ESP 2 also is well constrained. These data, like ESP 5, contain both pre-critical and post-critical reflections from Moho. The transition zone at this location (a velocity gradient from 7.65 to 8.0 km s^{-1}) is thicker (1.37 km), and the velocity discontinuity at its top is smaller (a jump from 7.05 to 7.65 km s^{-1}) than at the location ESP 5. The lower velocity discontinuity (8.0 to 8.1 km s^{-1}), however, not well constrained at ESP 2. ESP 4 data do not show pre-critical reflections from Moho, and therefore the upper velocity discontinuity is not well determined. However, the velocity gradient is very well constrained by the arrival times of the wide-angle Moho arrivals. These data require a 2.28-km-thick velocity gradient (from 7.15 to 8.05 km s^{-1}), thicker than at both the ESP 5 and ESP 2 locations.

The structures of the crust/mantle transitions that we have determined at these three locations are similar in the sense that they all have a velocity gradient bounded by velocity discontinuities above and below. A seismic velocity gradient representing crust/mantle transition in the Atlantic was inferred earlier also by Bunch & Kennett (1980) and Purdy (1983). Our data suggest that a regional variation in the crust/mantle transition can be resolved. From ESP 5 to ESP 2 then ESP 4 we note that the upper velocity discontinuity reduces in size, while the velocity gradient increases in thickness. The overall similarity of the crust/mantle transition at these ESPs may also suggest that serpentinization of the upper mantle is not an appropriate model for the low-velocity zone at ESP 5 as it seems unlikely that a crust/mantle transition at the base of a layer formed by serpentinized upper mantle would be so similar to one formed at the base of an igneous plutonic crustal rock unit.

CONCLUSIONS

Resolution of several important elements of crustal structure described above demanded detailed analysis of fine-scale features in the seismograms using traveltime inversion techniques extended to include low-velocity zones, and forward modelling of traveltimes and seismograms in the x-t and tau-p domains. The majority of seismic data available for study of lower oceanic crustal structure do not have sufficient spatial density to allow these features to be recognized, and it is hardly surprising then that low-velocity zones are not commonly interpreted to be parts of standard oceanic crustal sections. A low-velocity zone, such as that present at ESP 5, would be very difficult to detect using most of the conventional data. We would not, of course, claim that low-velocity zones are common features of the lower crust; but we do suggest that much of the available seismic refraction data lack sufficient resolution to detect such a feature, even if it were common. Our principal conclusions are as follows:

From the traveltime and amplitude analysis of ESP data in western N Atlantic, we find that the lower crust at ESP 5 contains a thick low-velocity zone in V_p and V_s velocities. This low-velocity zone is not a regional feature—analysis of ESPs 2 and 4, sampled with the same techniques, shows that a low-velocity zone in the lower crust does not exist at these other locations. A comparison of structure sections from

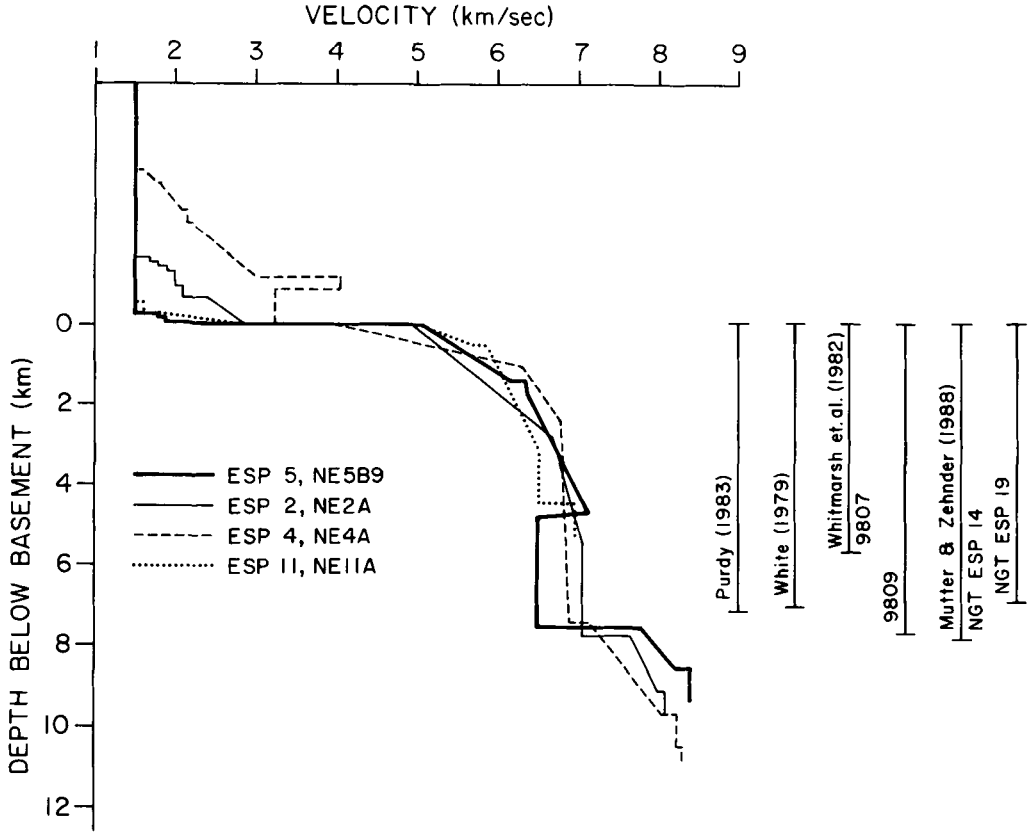

Figure 16. *P*-wave velocity functions derived from the analysis of NAT ESPs 5, 2, 4 and 11. All the velocity functions have been aligned at the interpreted sediments/crust interface. Notice that the thicknesses of the crust at the location of ESPs 5, 2 and 4 are remarkably similar, suggesting the low-velocity zone at the location of ESP 5 is altered crust, *not* altered upper mantle. Also shown are the crustal thickness results compiled from several earlier papers. These also suggest that the low-velocity zone is a part of the lower crust.

crust that displays a low-velocity zone and from crust that does not display such a low-velocity zone shows that the total crustal thickness in these differing cases is very similar, and from this we infer that that low-velocity zone at ESP 5 occurs within the crust, not underplate an otherwise normal section. This observation is further strengthened when we include N Atlantic crustal thickness results from several other studies.

Given the above observations we conclude that serpentinization of the upper mantle is not an important process in determining crust and upper mantle velocity structure along the transect of the western N Atlantic that we have studied, although local serpentinization due to fracture zone tectonics cannot be excluded.

Other conclusions that result from our study are that the crust/mantle transition at ESPs 5, 2 and 4 is not a sharp boundary, but a zone (1–2 km thick) consisting of a velocity gradient, bounded by velocity discontinuities both above and below it, and that in most of the lower crust Q_s is equal to Q_p. The latter is in contrast with a variety of studies that have concluded that Q_s is approximately one-half of Q_p.

ACKNOWLEDGMENTS

This work was supported by the Office of Naval Research, grants N00014-80-C0098 and N00014-84-C0132. Acquisition of the NAT data which this study draws upon was a joint project between the Bundesanstalt fur Geowissenschaften und Rohstoffe, Federal Republic of Germany; the Lamont–Doherty Geological Observatory of Columbia University; the University of Rhode Island's Graduate School of Oceanography, and the University of Texas at Austin. The success of this unique experiment depended upon the dedication of the numerous scientists and technicians involved, and that of the masters and crew of the S/V *Prospekta* and R/V *Moore*. We have used computer programs for tau-sum inversion written by John Diebold; for this inversion extended to include low-velocity zones, and for computing traveltime curves, and synthetic WKBJ seismograms written by Emilio Vera; and for computing reflectivity synthetic seismograms written or modified by Friedemann Wenzel, Peter Buhl, Gerhard Muller and Leonard Alsop. Discussions with Emilio Vera were very helpful. This paper has been reviewed by John Diebold, Emilio Vera and Carolyn Zehnder, and an earlier version also by Paul Richards and G. M. Purdy. This study was initiated while R. M. was a graduate student studying under the direction of Paul Stoffa. Lamont–Doherty Geological Observatory contribution number 4436.

REFERENCES

Aki, K. & Richards, P. G., 1980. *Quantitative Seismology: Theory and Methods*, W. H. Freeman & Co., San Francisco.

Bunch, A. W. H. & Kennett, B. L. N., 1980. The crustal structure of the Reykjanes Ridge at 59°30'N, *Geophys. J.R. astr. Soc.*, **61,** 141–166.

Cary, P. W. & Chapman, C. H., 1989. Waveform inversion of Expanding Spread Profile 5 from North Atlantic Transect, *J. Geophys. Res.*, **93,** 13575–13588.

Chapman, C. H., 1978. A new method for computing synthetic seismograms, *Geophys. J.R. astr. Soc.*, **54,** 481–518.

Chapman, C. H. & Orcutt, J. A., 1985. The computation of body wave synthetic seismograms in laterally homogeneous media, *Rev. Geophys.*, **23,** 105–163.

Chiang, C. S. & Detrick, R. S., 1985. The structure of the lower oceanic crust from synthetic seismogram modeling of near-vertical and wide-angle reflections and refractions near DSDP site 417 in the western North Atlantic (Abstract), *Eos, Trans. Am. Geophys. Un.*, **66,** 956.

Christensen, N. I., 1978. Ophiolites, seismic velocities, and ocean crustal structure, *Tectonophys.*, **47,** 131–157.

Christensen, N. I. & Salisbury, M. H., 1975. Structure and constitution of the lower oceanic crust, *Rev. Geophys. Space Phys.*, **13,** 57–86.

Christensen, N. I. & Smewing, J. D., 1981. Geology and seismic structure of northern section of the Oman ophiolite, *J. geophys. Res.*, **86,** 2545–2555.

Clague, D. A. & Straley, P. F., 1977. Petrologic nature of the oceanic Moho, *Geology*, **5,** 133–136.

Detrick, R. S., Buhl, P., Vera, E., Mutter, J., Orcutt, J., Madsen, J. & Brocher, T., 1987. Multichannel seismic imaging of a crustal magma chamber along the East Pacific Rise, *Nature*, **326,** 35–41.

Diebold, J. B. & Stoffa, P. L., 1981. The traveltime equation, tau-*p* mapping, and inversion of common midpoint data, *Geophysics*, **46,** 3, 238–254.

Diebold, J. B., Stoffa, P. L., Buhl, P. & Truchan, M., 1981. Venezuela basin crustal structure, *J. geophys. Res.*, **86,** 7901–7923.

Diebold, J. B., Stoffa, P. L. & LASE Study Group, 1988. A large aperture seismic experiment in the Baltimore Canyon Trough, in *The Geology of North America, I-2, The Atlantic continental margin*, eds Sheridan, R. S. & Grow, J., pp. 387–398, Geological Society of America, Boulder.

Diebold, J. B., 1989. Tau (p) analysis in one, two and three dimensions, in Analysis of seismic data in the tau-p domain, ed. Stoffa, P. L., D. Reidel Publishing Co., Dordrecht, Holland, in press.

Donnelly, T., Francheteau, J., Bryan, W., Robinson, P., Flower, M., Salisbury, M. *et al.*, 1979. *Init. Rep. Deep Sea Drill. Proj.*

Ewing, M., Woollard, G. P. & Vine, A. C., 1939. Geophysical investigations in the emerged and submerged Atlantic coastal plain, *Bull. geol. Soc. Am.*, **50,** 257–296.

Fox, P. J. & Stroup, J. B., 1981. The plutonic foundation of the oceanic crust, in *The Oceanic Lithosphere, The Sea,* VII, ed. Emiliani C., pp. 119–218.

Fuchs, K. & Muller, G., 1971. Computation of synthetic seismograms with the reflectivity method and comparison with observations, *Geophys. J.R. astr. Soc.*, **23,** 417–433.

Gardner, G. H. F., Gardner, L. W. & Gregory, A. R., 1974. Formation velocity and density—the diagonistic basics for stratigraphic traps, *Geophysics*, **39,** 6, 770–780.

Garmany, J., 1979. On the inversion of traveltimes, *Geophys. Res. Lett.*, **6,** 277–279.

Gerver, M. & Markushevich, V., 1966. Determination of a seismic wave velocity from the traveltime curve, *Geophys. J.R. astr. Soc.*, **11,** 165–173.

Hamilton, E. L., 1978. Sound velocity–density relations in sea-floor sediments and rocks, *J. acoust. Soc. Am.*, **63,** 366–377.

Huang, J. A., Chu, Y. H. & Kuo, J. T., 1986. Low velocity zone at base of oceanic crust: Exact inversion results of north Atlantic Transect ESP data (Abstract), *Eos,* **67,** 1110.

Kennett, B. L. N., 1974. Reflections, rays and reverberations, *Bull. seism. Soc. Am.*, **65,** 1643–1651.

Kent, D. V. & Gradstein, F. M., 1986. A Jurassic to Recent chronology, in *The Western Atlantic region,* vol. M, *The geology of North America,* eds Tucholke, B. E. & Vogt, P. R., pp. 45–50, Geological Society of America, Boulder.

LASE Study Group, 1986. Deep structure of the US East Coast passive margin from large aperture seismic experiments (LASE), *Marine Petrol. Geol.*, **3,** 234–242.

Lewis, B. T. R. & Snydsman, W. E., 1977. Evidence for a low-velocity layer at the base of oceanic crust, *Nature,* **266,** 340–344.

Lewis, B. T. R. & Snydsman, W. E., 1979. Fine structure of the lower oceanic crust on the Cocos plate, *Tectonophys.*, **55,** 87–105.

McCarthy, J., Mutter, J. C., Morton, J. L., Sleep, N. H. & Thompson, G. A., 1989. Relic magma chamber structures preserved within the Mesozoic North Atlantic crust?, *Bull. geol. Soc. Am.*, **100,** 1423–1436.

Mithal, R., 1986. Evidence for a basal low-velocity zone in oceanic crust, and new methods of phase analysis and extremal inversion, PhD thesis, Columbia University, New York.

Muller, G., 1985. The reflectivity method: a tutorial, *J. Geophys.*, **58,** 153–174.

Mutter, J. C., Talwani, M. & Stoffa, P. L., 1984. Evidence for a thick oceanic crust adjacent to the Norwegian margin, *J. geophys. Res.*, **89,** 483–502.

Mutter, J. C. & NAT Study Group, 1985. Multichannel seismic images of the oceanic crust's internal structure: Evidence for a magma chamber beneath the Mesozoic Mid-Atlantic Ridge, *Geology,* **13,** 629–632.

Mutter, J. C. & Zehnder, C. M., 1988. Deep crustal structure and magmatic processes: The inception of seafloor spreading in the Norwegian–Greenland sea, in *Early Tertiary Volcanism and the Opening of the NE Atlantic,* eds Morton, A.C. & Parson, L. M., *Geol. Society,* S.P., **39,** 35–48.

NAT Study Group, 1985. North Atlantic Transect: A wide-aperture, two-ship multichannel seismic investigation of the oceanic crust, *J. geophys. Res.*, **90,** 10321–10341.

Nichols, G. M., Warren, N., Luyendyk, B. P. & Spudich, P., 1980. Seismic velocity structure of the ophiolite at Point Sal, southern California, determined from laboratory measurements, *Geophys. J.R. astr. Soc.*, **63,** 165–185.

Orcutt, J. A., 1980. Joint linear, extremal inversion of seismic kinematic data, *J. geophys. Res.*, **85,** 2649–2660.

Purdy, G. M., 1983. The seismic structure of 140 Myr old crust in the western central Atlantic ocean, *Geophys. J.R. astr. Soc.*, **72,** 115–137.

Salisbury, M. H., 1974. Investigations of seismic velocities in the Bay of Islands, Newfoundland ophiolite complex for comparison with oceanic seismic structure, *PhD thesis, University of Washington,* Seattle.

Salisbury, M. H. & Christensen, N. I., 1978. The seismic velocity structure of a traverse through the Bay of Islands ophiolite complex, New Foundland, an exposure of oceanic crust and upper mantle, *J. geophys. Res.*, **83,** 805–817.

Salisbury, M. H., Scott, J. H., Auroux, C. A. *et al.*, 1986. *Proc. Initial Reports (Pt A)*, Ocean drilling Program, 102.

Schouten, H. & Klitgord, K. D., 1977. Map showing magnetic anomalies, western North Atlantic, *U.S. geol. Surv. misc. Field Stud. Map, MF-915.*

Spudich, P. & Orcutt, J. A., 1980a. Petrology and porosity of an oceanic crustal site: Results from waveform modeling of seismic refraction data, *J. geophys. Res.*, **85,** 1409–1433.

Spudich, P. & Orcutt, J. A., 1980b. A new look at the seismic velocity structure of the oceanic crust, *Rev. Geophys. Space Phys.*, **18,** 627–645.

Spudich, P., Salisbury, M. H. & Orcutt, J. A., 1978. Ophiolites found in oceanic crust?, *Geophys. Res. Lett.*, **5,** 341–344.

Stoffa, P. L. & Buhl, P., 1979. Two-ship multichannel seismic experiments for deep crustal studies: Expanded spread and constant offset profiles, *J. geophys. Res.*, **84,** 7645–7660.

Stoffa, P. L., Buhl, P., Diebold, J. B. & Wenzel, F., 1981. Direct mapping of seismic data to the domain of intercept time and ray parameter: A plane wave decomposition, *Geophysics,* **46,** 255–267.

Vera, E. E. & Diebold, J. B., 1984. Generalized inversions of discrete tau-*p* data (Abstract), *Eos,* **65,** 239.

Watts, A. B., ten-Brink, U., Buhl, P. & Brocher, T. M., 1985. A multichannel seismic study of lithospheric flexture across the Hawaiin-Emperor seamount chain, *Nature,* **315,** 105–111.

Wenzel, F., Stoffa, P. L. & Buhl, P., 1982. Seismic modeling in the domain of intercept time and ray parameter, IEEE Trans. *Acoustic Speech Signal Process.*, **30,** 406–423.

White, R. S., 1979. Oceanic upper crustal structure from variable angle seismic reflection–refraction profiles, *Geophys. J.R. astr. Soc.*, **57,** 683–726.

White, R. S., 1984. Atlantic ocean crust: seismic structure of a slow spreading ridge, in *Ophiolites and Oceanic Lithosphere*, eds. Gass, I. G., Lippard, S. J. & Shelton, A. W., pp. 101–111, Geological Society of London.

White, R. S., Spence, G. D., Fowler, S. R., McKenzie, D. P., Westbrook, G. K. & Bowen, A. N., 1987. Magmatism at rifted continental margins, *Nature*, **330,** 439–444.

Whitmarsh, R. B., Ginsburg, A. & Searl, R. C., 1982. The structure and origin of the Azores–Biscay Rise, North-east Atlantic ocean, *Geophys. J.R. astr. Soc.*, **70,** 79–107.